Cell autonomous and cell non-autonomous effects of mosaic Mecp2 expression on layer V pyramidal cell morphology in a mouse model of Rett Syndrome

by

Leslie A. Rietveld
B.Sc., The King's University College, 2008

A Thesis Submitted in Partial Fulfillment
of the Requirements for the Degree of

MASTER OF SCIENCE

in the Department of Biology

Supervisory Committee

Cell autonomous and cell non-autonomous effects of mosaic Mecp2 expression on layer V pyramidal cell morphology in a mouse model of Rett Syndrome

by

Leslie A. Rietveld
B.Sc., The King's University College, 2008

Supervisory Committee

Dr. Kerry R. Delaney, Co-supervisor
(Department of Biology)

Dr. Patrick Nahirney, Co-supervisor
(Department of Biology)

Dr. Perry L. Howard, Departmental Member
(Department of Biology)

Abstract

Supervisory Committee

Dr. Kerry R. Delaney, Co-supervisor
(Department of Biology)

Dr. Patrick Nahirney, Co-supervisor
(Department of Biology)

Dr. Perry L. Howard, Departmental Member
(Department of Biology)

Rett Syndrome (RTT) is a neurodevelopmental disorder primarily caused by mutations in the X-linked gene methyl-CpG-binding protein 2 (*MECP2*). The mosaic brain environment in heterozygous (*MECP2*$^{+/-}$*)* females consists of both MeCP2-wildtype (MeCP2+) and Mecp2-mutant (MeCP2-) neurons. To separate possible cell autonomous and cell non-autonomous effects three-dimensional morphological analysis was performed on individually genotyped layer V pyramidal neurons in the primary motor cortex of heterozygous (*Mecp2*$^{+/-}$) and wild-type (*Mecp2*$^{+/+}$) mature female mice (>8 months old) from the *Mecp2*$^{tm1.1Jae}$ line. Mecp2$^{+/+}$ neurons and Mecp2+ were found to be indistinguishable while Mecp2- neurons have significantly reduced basal dendritic length ($p<0.05$), predominantly in the region 70-130 μm from the cell body, culminating in a total reduction of 15%. Mecp2- neurons have three (17%) fewer total branch points, lost specifically at the second and third branch orders. Thus the reduced total dendritic length in Mecp2- neurons is a result of fewer higher-order branches. Soma and nuclear areas of 30 *Mecp2*$^{+/-}$ female mice (5-21 months) with X chromosome inactivation (XCI) ratios ranging from 12% to 56% were analyzed. On average Mecp2- somata and nuclei were 15% and 13% smaller than Mecp2+ neurons respectively. The variation observed in the soma and nuclear sizes of Mecp2- neurons was not due to age, but was found to be correlated with the XCI ratio. Animals with a balanced XCI ratio (approximately 50% Mecp2-) were found to have Mecp2- neurons with a less severe cellular phenotype (11-17% smaller than Mecp2+). Animals with a highly skewed XCI ratio favouring expression of the wild-type allele (less than 30% Mecp2-) were found to have a more severe Mecp2- cellular phenotype (17-22% smaller than Mecp2+). These data support indicate that mutations in *Mecp2* exert both cell autonomous and cell non- autonomous effects on neuronal morphology.

Table of Contents

List of Tables

List of Figures

List of Abbreviations

CDKL5	Cyclin-dependent kinase-like 5
CTD	C-terminal domain
DAPI	4,6-diamidino-2-phenylindole
GFP	Green fluorescent protein
H1	Histone 1
HDAC	Histone deacetylase
MAP-2	Microtubule-associated protein 2
MBD	Methyl-CpG binding domain
Mecp2	Methyl-CpG binding protein 2
Mecp2$^{+/+}$	Wild-type female mouse
Mecp2$^{+/-}$	Heterozygous female mouse
Mecp2$^{-/y}$	Hemizygous male mouse
Mecp2+	Neurons expressing wild-type Mecp2 in a heterozygous female
Mecp2-	Neurons expressing mutant Mecp2 in a heterozygous female
n.a.	Numerical aperture
NLS	Nuclear localization signal
RTT	Rett syndrome
TRD	Transcriptional repressor domain
UTR	Untranslated region
WW	WW domain binding region
XCI	X chromosome inactivation
YFP	Yellow fluorescent protein

Acknowledgments

I would like to thank Dr. Kerry Delaney for the opportunity to work in his lab and his generous support during this thesis project. I would also like my committee members Drs. Perry Howard and Patrick Nahirney for their guidance and helpful suggestions. My sincerest thanks also goes to David Stuss, whose advice, insightful criticisms, and kind encouragement were indispensible throughout the entirety of my project. I would also like to thank Veronika Losonczi and Laura Tebb for their tireless imaging and tracing of neurons. I am also thankful for the technical support provided by Richard Taylor and David McPhee. Finally I would like to thank all the members of the Delaney, Nashmi, and Chow labs for their friendship and kindness along the way.

Dedication

This thesis is dedicated to my parents, Floyd and Tracie, for their love and encouragement and to Douglas, whose inquisitiveness continues to inspire my own.

Chapter 1 – Introduction

1.1 Rett Syndrome

Rett Syndrome (RTT; MIM 312750) is a neurodevelopmental autism spectrum disorder that was first characterized by Andreas Rett in 1966 (Rett, 1966). It has been found to affect one in 10,000 females (Laurvick et al., 2006) with typical RTT patients being diagnosed after a period of normal development (six to eighteen months of age), followed by a period of regression marked by four main criteria: partial or complete loss of purposeful hand movements, development of gait abnormalities, loss of verbal language skills and the presence of stereotypic hand movements (Neul et al., 2010). RTT patients also exhibit decreased head circumference, although there are no other notable facial abnormalities (Allanson et al., 2011). Atypical RTT is differentiated by meeting only two of the four main criteria stated above for typical RTT and five of these eleven supportive criteria: breathing disturbances, bruxism, impaired sleep patterns, abnormal muscle tone, peripheral vasomotor differences, scoliosis/kyphosis, slowed growth, small cold hands and feet, inappropriate laughing/screaming spells, reduced pain response, and eye pointing (Neul et al., 2010). Despite the numerous severe symptoms associated with RTT, survival rate at 25 years of age is 78% (Laurvick et al., 2006) with some patients surviving well into their sixties (Hagberg, 2005; Freilinger et al., 2010; Kirby et al., 2010). Some behavioural deficits in RTT have been shown to improve through life (Zappella et al., 2003), although other studies have shown that phenotypes are consistent across the lifespan of individuals (Kaufmann et al., 2011).

1.1.1 Genetic cause of RTT – Mutations in *MECP2* and *CDKL5*

The majority of females with typical RTT are heterozygous for a mutation in the X-linked gene methyl-CpG-binding protein 2 (*MECP2*)(Figure 1) (Amir et al., 1999; Archer et al., 2006). Most *MECP2* mutations in RTT patients are caused by *de novo* germline mutations transmitted paternally (Trappe et al., 2001). Over 2000 mutations have been characterized along the entire length of the gene, including nonsense, missense,

frameshift, and large truncation mutations (Philippe et al., 2006; Weaving et al., 2005; Amir and Zoghbi, 2000). Eight common missense mutations at CpG dinucleotides account for 65% of the reported cases of RTT (Miltenberger-Miltenyi and Laccone, 2003) and lead to a loss of function of MeCP2 due to unstable, truncated, or improperly folded proteins (Bienvenu and Chelly, 2006). Phenotype genotype studies have found that early truncation mutations close to the N-terminal end of the protein have been correlated with a more severe phenotype (typical RTT) than late truncation mutations near the C-terminal end of the protein (Zappella et al., 2001; Charman et al., 2005). Over 50% of atypical RTT patients have no mutation in the gene *MECP2* (Archer et al., 2006), although mutations in the X-linked gene cyclin-dependent kinase-like 5 (*CDKL5)* have been implicated in some of these cases (Weaving et al., 2004; Tao et al., 2004; Mari et al., 2005). Cdkl5 and Mecp2 have been found in mice to interact *in vivo* and *in vitro*, with similar spatio-temporal expression patterns (Mari et al., 2005), which may explain how mutations in these two genes can lead to similar phenotypes. Over expression of MeCP2 in humans has also been shown to cause developmental delays similar to those seen in RTT suggesting that proper expression of MeCP2 is critical to neurodevelopment (Prescott et al., 2009; Campos et al., 2010).

1.1.2 MeCP2 structure

The protein encoded by the *MECP2* gene has five domains (Figure 1); a highly conserved methyl-CpG binding domain (MDB) (Meehan et al., 1992) characteristic of its protein family, a transcriptional repressor domain (TRD) which interacts with histone deacetylases 1 and 2 (HDAC1 and HDAC2) (Nan et al., 1997; Jones et al., 1998; Nan et al., 1998; Kokura et al., 2001), a nuclear localization signal (NLS) (Nan et al., 1996), a C-terminal domain (CTD) which contributes to DNA-binding (Chandler et al., 1999), and a proline rich WW domain binding region (PR) that aids in protein-protein interactions (Buschdorf and Strätling, 2004). The four exons of *MECP2* are alternatively spliced into MeCP2_e1 and MeCP2_e2 transcripts, which are characterized by containing either exon 1 (MeCP2_e1) or exon 2 (MeCP2_e2) in their 5' region with all downstream domains intact (Kriaucionis and Bird, 2004; Mnatzakanian et al., 2004). Additionally, MeCP2_e1

has a long 3' untranslated region (UTR) that contains multiple microRNA recognition elements (Klein et al., 2007). The tertiary structure of MeCP2 contains many highly disordered regions, a common characteristic among eukaryotic transcription factors (Adams et al., 2007; Liu and Francke, 2006).

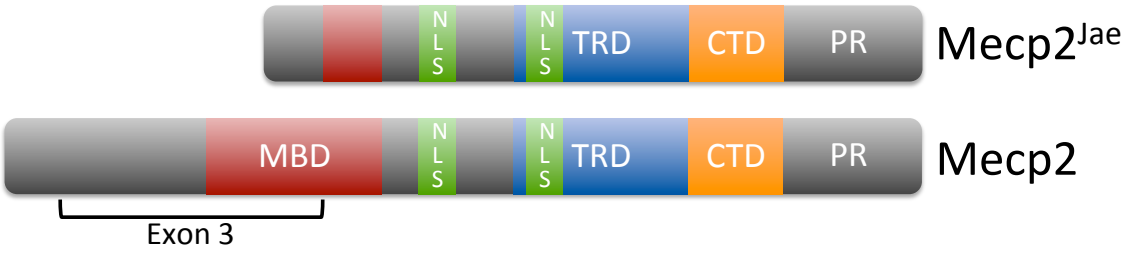

Figure 1. Structure of wild-type Mecp2 and mutant Mecp2^{Jae}. Mecp2 contains a MBD that binds to methylated DNA, a TRD that interacts with HDACs to repress transcription, a NLS that directs the protein to the nucleus, a CTD that binds unmethylated DNA, and a PR region that interacts with WW domains of other proteins. *Mecp2^{Jae}* has exon three deleted, which comprises most of the MBD. The resulting translated mutant protein may be partly functional, leading to a milder phenotype in animals expressing Mecp2^{Jae}.

1.1.3 MeCP2 expression and function

Recent research in mice indicates that Mecp2 is found in many tissue types, but it is most abundant in the brain, with neuronal nuclei having ten times higher expression of Mecp2 than glial nuclei (Skene et al., 2010). The Mecp2_e1 isoform is also ten times more abundant in the brain of humans and mice than Mecp2_e2 (Kriaucionis and Bird, 2004; Mnatzakanian et al., 2004; Dragich et al., 2007), however either isoform has been found to rescue a mutant phenotype in mice (Kerr et al., 2011). Mecp2 is found within the heterochromatic regions in the nucleus but it disperses throughout the nucleus when the levels of DNA methylation are low (Nan et al., 1996). Low levels of Mecp2 have also been detected in the post synaptic compartment (Aber et al., 2003). Mecp2 expression levels are low prenatally, but increase after birth during the final stages of neurogenesis (Kishi and Macklis, 2004; Skene et al., 2010; Balmer et al., 2003), where Mecp2

contributes to neuronal dendritic maturation (Kishi and Macklis, 2004) and synaptogenesis (Fukuda et al., 2005; Armstrong 1995).

Methylated DNA is associated with transcriptional repression; therefore the first functional studies of Mecp2 investigated it as global repressor of transcription. It was found that the TRD of Mecp2 acts with the corepressor complex Sin3A (including HDAC1 and HDAC2) to remodel chromatin, impeding access of the transcriptional machinery thereby repressing gene expression (Nan et al., 1997; Nan et al., 1998). Mecp2 facilitated repression of genes is responsible for reducing transcriptional noise, and if Mecp2 is knocked-out, levels of histone acetylation increase, resulting in an abundance of transcripts (Skene et al., 2010; Shahbazian et al., 2002). The CTD of Mecp2 binds unmethylated DNA which facilitates long-range chromatin compaction (Georgel et al., 2003; Nikitina et al., 2007; Horike et al., 2005). Mecp2 also links peripheral heterochromatin to the nuclear envelope, aiding in assembly of the nuclear envelope and cell proliferation (Babbio et al., 2012).

Microarray and chromatin immunoprecipitation studies of Mecp2 knockout and overexpression models have revealed that 85% (approximately 2400) of affected genes were down-regulated in the knockout and up-regulated in the overexpression model, indicating that Mecp2 also acts as an activator of transcription (Ben-Shachar et al., 2009; Chahrour et al., 2008; Yasui et al., 2007). Mecp2 mediated transcriptional activation occurs through interactions with the transcriptional activator cAMP response element-binding protein (CREB) (Chahrour et al., 2008). Mecp2 has also been implicated in the regulation of alternate RNA splicing by binding to RNA directly but also through interactions with the RNA binding Y-box binding protein 1 (Young et al., 2005). The multiple microRNA recognition elements of Mecp2_e1 include a binding site for miR132, which has been found to regulate the translation of Mecp2 (Vo et al., 2005; Wayman et al., 2008; Klein et al., 2007).

Mecp2 function is modified by several activity dependent post-translational modifications. The phosphorylation of serine 421 on Mecp2 has been found to be

initiated by an influx of calcium ions associated with increased neuronal activity (Chen et al., 2003), leading to derepression of gene targets such as brain-derived neurotrophic factor (Zhou et al., 2006), localization of Mecp2 to the nucleus during differentiation (Miyake and Nagai, 2007) and genome-wide chromatin regulation (Cohen et al., 2011). Activity dependent dephosphorylation of serine 80 has also been found to be important for chromatin-Mecp2 associations (Tao et al., 2009). Epigenetic modifications such as DNA methylation are dynamic and may lead to highly variable Mecp2 binding across the genome of individuals during differentiation, development, and aging (Kangaspeska et al., 2008).

1.1.4 X chromosome inactivation

MECP2 is located on the X chromosome and therefore it is affected by X chromosome inactivation (XCI) (Adler et al., 1995; Ross et al., 2005). XCI is the process by which the majority of genes on one X chromosome in XX females are silenced thereby equalizing gene dosage to that of XY males (Lyon, 1961; Carrel and Willard, 2005). XCI occurs in early embryogenesis (gastrulation in humans), randomly inactivating either the maternal or paternal X chromosome in each cell, passing the status onto all progeny (Figure 2) (Bermejo-Alvarez et al., 2012). XCI results in a similar number of maternal and paternal X chromosome expressing cells (50:50) in the majority of human females, with approximately 9% having skewed ratios (80:20), and less than 1% having extremely skewed ratios (95:5) (Amos-Landgraf et al., 2006). Increased rates of XCI skewing have been reported to correlate with increasing age in human females (Bittel et al., 2008) and Mecp2 mutant animals (Metcalf et al., 2006). Age-dependent increases in skewed XCI ratios are not caused by a gradual selection over time but are the result of an abrupt shift in the number of cells expressing each chromosome (Sandovici et al., 2004).

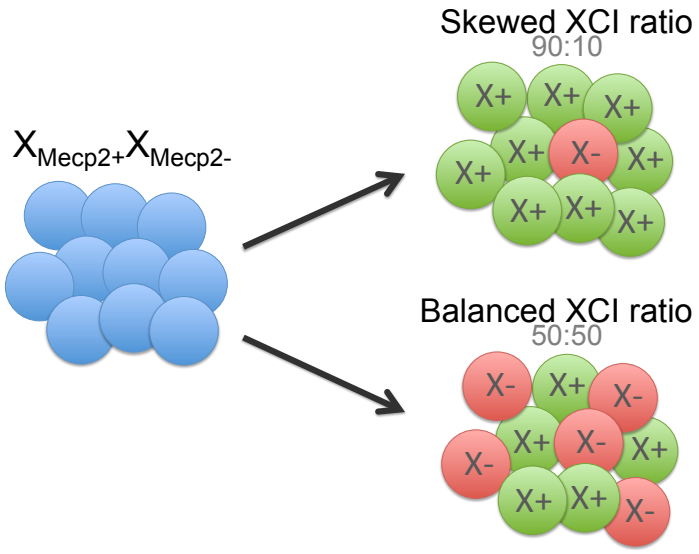

Figure 2. Random and non-random XCI. Early in embryogenesis cells undergo XCI, resulting in either the maternal or paternal X chromosome being inactivated. This process normally results in a balanced number of cells expressing each X chromosome, but rarely one X chromosome may be preferentially inactivated leading to a skewed ratio. Skewed ratios always favour inactivation of the mutant X chromosome. X+ = X chromosome with wild-type Mecp2 active, X- = X chromosome with mutant Mecp2 active. Derived in part from (Minks and Brown, 2009).

XCI results in two populations of cells in RTT females, those expressing wild-type MeCP2 (MeCP2+), and those either lacking MeCP2 or expressing a mutant form of the protein (MeCP2-). Although the majority of patients with typical RTT have balanced XCI ratios (Shahbazian et al., 2002), the rate of skewed XCI ratios, always favouring inactivation of the mutant X chromosome, is much higher in patients with X-linked disorders such as RTT than in the general population (Belmont, 1996; Brown and Robinson, 2000; Puck, and Willard, 1998; Plenge et al., 2002; Young and Zoghbi, 2004). The proportion of MeCP2- expressing cells in *MECP2*$^{+/-}$ females has been found to be positively correlated with phenotype severity (Archer et al., 2007; Chae et al., 2004). However skewed XCI ratios have not been able to account for the phenotype variability observed between RTT females with identical mutations in *MECP2*, suggesting other epigenetic factors may also be influencing phenotype (Ishii et al., 2001). Extremely

skewed XCI ratios have been found in the rare female carriers of a *MECP2* mutation presenting with no RTT symptoms (Amir et al., 2000; Weaving et al., 2005; Miltenberger-Miltenyi and Laccone, 2003; Young and Zoghbi, 2004; Plenge et al., 2002; Sirianni et al., 1998). In contrast skewed XCI ratios in mice have not been correlated with asymptomatic phenotypes, although they have been found to contribute to phenotype variability (Samaco et al., 2012). XCI ratios are, however, variable across tissue types and brain regions (Young and Zoghbi, 2004), with the blood having the most highly skewed ratio (Gale et al., 1994; Sharp et al., 2000), therefore XCI ratios taken from the blood may not accurately reflect the ratios in the brain. This indicates that correlations made between XCI ratios found in non-brain tissue and RTT symptom severity may be prone to extreme error.

1.2 Neocortical neuropathology of RTT

RTT patients deficient in MeCP2 have been shown to have reductions in the volume of grey matter in the frontal and temporal lobes, caudate nucleus, thalamus, midbrain, and cerebellum (Reiss et al., 1993; Casanova et al., 1991; Subramaniam et al., 1997). Reductions in the volume of grey matter in the frontal and temporal lobes have been found to be predictive of phenotype severity in RTT (Carter et al., 2008). Neurodegeneration has not been observed, indicating that RTT is primarily a neurodevelopmental disorder (Jellinger and Seitelberger, 1986; Jellinger et al., 1988; Armstrong, 1995). Morphological studies performed on post-mortem tissue from RTT patients have revealed that the reduction in brain volume is due to increased neuron density and reductions in neuronal cell body size (Bauman et al., 1995). It has also been found that RTT patients have reduced dendritic arborization and spine density of layer II/III and V/VI pyramidal cells in the frontal and temporal areas (Belichenko et al., 1994; Belichenko et al., 1997) including the motor cortex (Armstrong, 1995)(see below for a detailed description of the neocortex). Similar reductions in spine density have been found in hippocampal CAI neurons of RTT patients (Chapleau et al., 2009). In the rare male cases of RTT, reductions in layer III and V basal and apical dendritic morphology have also been observed (Schüle et al., 2008).

1.2.1 Neocortical organization

The neocortex consists of six distinct cell layers. Pyramidal neurons constitute about 70% of the total cells in the neocortex and are distinguished from non-pyramidal neurons by containing: spiny dendrites, an apical dendrite which forms a tuft in layer I, basal dendrites, a subcortically projecting axon with collaterals projecting intracortically, asymmetric synaptic contacts, and the excitatory neurotransmitter glutamate (reviewed in Nieuwenhuys, 1994). Pyramidal neurons are the main excitatory cell in all layers except layer IV, which contains spiny stellate neurons that lack an apical dendrite (Watts and Thomson, 2005). The sparsely populated layer I contains GABAergic neurons only and the apical tufts of pyramidal neurons (Nieuwenhuys, 1994). Layer II/III contains mostly pyramidal neurons, which send projections within layer II/III and to layer V (Thomson et al., 2002). Layer IV basket and spiny stellate cells receive thalamic input (Ahmed et al., 1994; Ahmed et al., 1997) and pyramidal and spiny stellate cells send out projections within layer IV and to layers III, V, and VI (Parnavelas et al., 1977; Burkhalter and Bernardo, 1989; Anderson et al., 1994). Layer V contains the largest pyramidal cells, which project to all cortical layers (Burkhalter and Bernardo, 1989). Layer VI pyramidal neurons receive input from the thalamus, although at a much lower level than layer IV, and have both thalamic and cortical projections (Bannister, 2005). In summary information is sent from the thalamus to layer IV, passed from layer IV to layer II/III, further relayed from layer II/III to V, and then sent from layer V to layer VI and other subcortical targets (Gilbert, 1993).

1.3 *Mecp2* mutant mouse models

Since the discovery of the link between *MECP2* and RTT (Amir and Zoghbi, 2000), many genetically modified mouse lines have been generated to model the RTT phenotype and investigate the role of MeCP2 in the brain. One of the first *Mecp2* knockout mouse lines generated had exons three and four excised ($Mecp2^{Bird}$), resulting in a severe phenotype due a complete lack of Mecp2 expression (Guy et al., 2001). Most RTT cases are caused by missense mutations resulting in the production of a mutant protein (Miltenberger-Miltenyi and Laccone, 2003), therefore RTT mouse models

expressing a mutant protein were generated, either by the insertion of a premature stop codon at the C-terminal end (*Mecp2*^{308}) (Shahbazian et al., 2002), or by the deletion of exon three near the N-terminal (*Mecp2*^{Jae}) (Chen et al., 2001). *Mecp2* has also been selectively knocked out in the forebrain (Chen et al., 2001), in Sim1-positive neurons in the hypothalamus (Fyffe et al., 2008), in tyrosine hydroxylase positive neurons (Samaco et al., 2009), and in GABAergic neurons in the forebrain of mice (Chao et al., 2010) to identify the specific targets of Mecp2.

Mecp2^{Jae} mice have exon three of *Mecp2* excised, which constitutes most of the MBD on the N-terminal end of the protein (Figure 1) (Chen et al., 2001). Due to the varying degree of mutation of *Mecp2* in the mouse models, *Mecp2*^{Jae} mice have a less severe phenotype than *Mecp2*^{Bird} (Guy et al., 2001; Belichenko et al., 2008) but a more severe phenotype than *Mecp2*^{308} (Shahbazian et al., 2002) which makes them ideal for the study of symptomatic female *Mecp2*$^{+/-}$ mice into late adulthood.

1.3.1 Overview of morphological and functional deficiencies in *Mecp2*$^{-/y}$ mice

Most research has involved the use of *Mecp2* mutant male mice (*Mecp2*$^{-/y}$) as their symptom onset and disease progression more closely mirrors RTT patients than female *Mecp2*$^{+/-}$ mice. *Mecp2*$^{-/y}$ mice express mutant Mecp2 in all their cells making initial studies less complex as they did not have to consider the genotypically heterogeneous population of cells created by XCI. *Mecp2*$^{-/y}$ mutant mice display (to varying degrees depending on mutation) many symptoms characteristic of RTT such as hypoactivity, kyphosis, gait abnormalities, hind-limb clasping, decreased body and brain weight, tremors, seizures, and strained breathing starting at around six weeks of age (Chen et al., 2001; Guy et al., 2001; Shahbazian et al., 2002).

Mecp2$^{-/y}$ mice display a similar reduction in cortical volume to that observed in RTT patients (Fukuda et al., 2005; Saywell et al., 2006; Belichenko et al., 2008). Cortical layers II/III and V/VI are the most severely reduced in thickness, with no observable reduction in layer IV thickness (Kishi and Macklis, 2004). Increased neuronal density and

reduced somata and nuclear sizes in layers II/III, IV, and V/VI of the neocortex has also been reported in *Mecp2*$^{-/y}$ mice (Fukuda et al., 2005; Kishi and Macklis, 2004; Chen et al., 2001). Dendritic spines in *Mecp2*$^{-/y}$ mice are swollen and less numerous in the motor cortex, fascia dentate, and CA1 and dentate gyrus of the hippocampus (Belichenko et al., 2009; Smrt et al., 2007; Stuss et al., 2012). Recently it has been found that in pre-symptomatic *Mecp2*$^{-/y}$ mice (P7) CA1 neurons in the hippocampus have reduced spine density, however when symptoms appear (P15), the spine density is the same as wild-type mice (Chapleau et al., 2012). Axonal targeting is also disrupted in Mecp2 deficient mice (Belichenko et al., 2009; Matarazzo et al., 2004). Pyramidal neurons in cortical layers II/III and V are also smaller and less complex in *Mecp2*$^{-/y}$ mice (Kishi and Macklis, 2004; Stuss et al., 2012).

Interestingly the majority of these phenotypes can be prevented upon reactivation of the *Mecp2* gene before symptom onset, and reversed upon reactivation of *Mecp2* after the onset of symptoms (Guy et al., 2007; Luikenhuis et al., 2004; Jugloff et al., 2008; Robinson et al., 2012). Additionally, inactivation of *Mecp2* in adult mice can cause similar phenotypes, indicating that expression of Mecp2 is not just important during development but is vital for proper brain aging (Cheval et al., 2012; McGraw et al., 2011). Overexpression of Mecp2 in mice also produces a similar phenotype to those observed in RTT mouse models (Collins et al., 2004) signifying that precise regulation of the levels of Mecp2 expression is essential for healthy brain function in mice.

1.3.2 Phenotype of *Mecp2*$^{+/-}$ mice

Mecp2$^{+/-}$ female mice more accurately model RTT syndrome as they recapitulate the mosaic brain environment created by XCI. The progression of symptoms in *Mecp2*$^{+/-}$ mice is notably slower than in *Mecp2*$^{-/y}$ mice. *Mecp2*$^{+/-}$ mice display the same RTT-like neurodevelopmental and motor abnormalities as *Mecp2*$^{-/y}$ but they normally appear at six months of age with some mice living a normal lifespan (Guy et al., 2001; Chen et al., 2001; Guy et al., 2007; Bissonnette and Knopp, 2006; Bissonnette and Knopp, 2008; Abdala et al., 2010; Bissonnette et al., 2007). Recently, however, progressive motor

deficits, reduced anxiety, apnea, and weight gain have been described in seemingly pre-symptomatic *Mecp2*$^{+/-}$ mice as young as three to four weeks (Santos et al., 2007; Samaco et al., 2012).

1.3.3 Cell autonomous and cell non-autonomous morphological deficits in *Mecp2*$^{+/-}$ mice

Due to XCI, the brains of female *Mecp2* mutant mice have two genotypically distinct cell types: cells expressing wild-type Mecp2 (Mecp2+) and those expressing mutant Mecp2 (Mecp2-). This mosaic brain environment raises the question of whether the cellular phenotypes of Mecp2+ and Mecp2- neurons are determined by their individual genotype (cell autonomy) or by the environment or non-neuronal cells surrounding the neurons (cell non-autonomy). If Mecp2 acts in a solely cell autonomous manner (Figure 3B), then Mecp2+ neurons would resemble those of a wild-type female (*Mecp2*$^{+/+}$), and Mecp2- neurons would resemble those of a mutant male (*Mecp2*$^{-/y}$). Mecp2 has been found to act cell autonomously to affect the neuronal morphology of Mecp2- neurons in the substantia nigra (Gantz et al., 2011), layers II/III in the cortex (Kishi and Macklis, 2009), locus ceruleus (Taneja et al., 2009), and hippocampus (Chapleau et al., 2009). The nuclear size of Mecp2 deficient neurons has also been found to be reduced cell autonomously *in vitro* (Yazdani et al., 2012).

If Mecp2 acts in a cell non-autonomous manner (Figure 3C-F), then Mecp2- and Mecp2+ neurons would resemble *Mecp2*$^{+/+}$ neurons (beneficial environmental effect: Figure 3C), or Mecp2- and Mecp2+ neurons would resemble *Mecp2*$^{-/y}$ neurons (deleterious environmental effect: Figure 3D). Beneficial and deleterious environmental effects may be caused by the surrounding non-neuronal cells in the brain. Many other possible outcomes could be predicted based on cell autonomous effects coupled with cell non-autonomous effects: Mecp2+ neurons could be larger than both Mecp2- and *Mecp2*$^{+/+}$ neurons (compensation: Figure 3E), or Mecp2- neurons could be smaller than *Mecp2*$^{-/y}$ neurons and Mecp2+ could be larger than *Mecp2*$^{+/+}$ (competition: Figure 3F). Compensation and competition cell non-autonomous effects could stem from neuron-

neuron interactions such as activity-dependent neuronal maturation (Zhou et al., 2006; Singleton et al., 2011; Cohen et al., 2011).

The non-neuronal environment in the brain, which consists primarily of glia, can have cell non-autonomous effects on neuronal morphology. Although previous research claimed that glia do not express Mecp2 (Shahbazian et al., 2002), recent studies have determined that astrocytes, microglia and oligodendrocytes all express Mecp2 to varying degrees (Maezawa et al., 2009; Ballas et al., 2009; Maezawa and Jin, 2010). Mecp2 deficiency leads to early and accelerated gliogenesis, which can impact proper neuronal development (Okabe et al., 2010). Mecp2 deficient astrocytes have been shown to cause cell non-autonomous reductions in the dendritic arborization of Mecp2+ neurons *in vitro* (Ballas et al., 2009; Maezawa et al., 2009). Mecp2- microglia and astrocytes contribute to impaired neuronal morphology by releasing high levels of glutamate, which is toxic to Mecp2+ and Mecp2- neurons (Maezawa and Jin, 2010; Okabe et al., 2012). The important role glia play in the RTT phenotype has been demonstrated by the amelioration of some key phenotypes (locomotion, anxiety, respiratory abnormalities, and lifespan) of Mecp2 mutant mice upon re-expression of Mecp2 in astrocytes (Lioy et al., 2011) and microglia (Derecki et al., 2012). The severity of cell non-autonomous effects can also be influenced by the proportion of Mecp2- and Mecp2+ cells in the brain (balanced vs. skewed XCI ratio). It has been shown that as the number of Mecp2- neurons in the female *Mecp2*$^{+/-}$ brain increases, the expression of Mecp2 in Mecp2+ neurons decreases proportionally (Braunschweig et al., 2004), suggesting that Mecp2+ neurons are negatively impacted by Mecp2- neurons and/or glia.

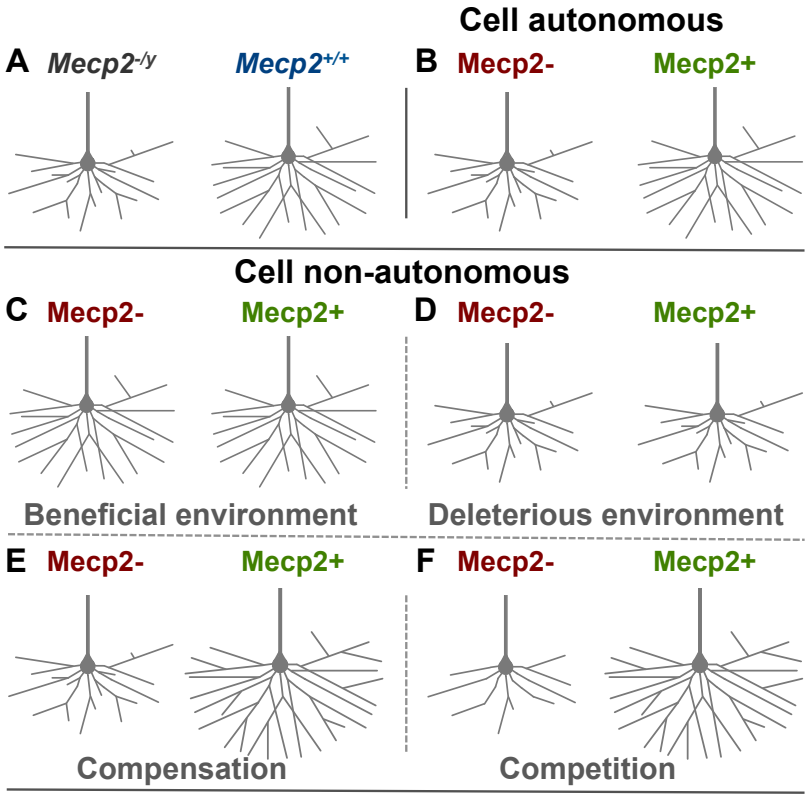

Figure 3. Possible cell autonomous and cell non-autonomous effects on neuronal morphology. (A) *Mecp2*$^{-/y}$ neurons represent the complete mutant neuronal phenotype. *Mecp2*$^{+/+}$ neurons represent the complete wild-type neuronal phenotype. **(B)** Cell autonomous effects of mutant Mecp2 in a *Mecp2*$^{+/-}$ female mouse would result in Mecp2- neuronal morphology resembling *Mecp2*$^{-/y}$, and Mecp2+ neuronal morphology resembling *Mecp2*$^{+/+}$ neurons, as their phenotypes would be determined by their cellular genotype alone. **(C)** Cell non-autonomous effects of mutant Mecp2 expression could result in Mecp2+ and Mecp2- neurons resembling *Mecp2*$^{+/+}$ if Mecp2+ neurons/glia are contributing to a beneficial environment for both neuronal genotypes. **(D)** Deleterious environmental cell non-autonomous effects could be triggered by harmful factors released from Mecp2- neurons/glia, resulting in Mecp2- and Mecp2+ neuronal morphologies resembling *Mecp2*$^{-/y}$. **(E)** Cell autonomous and cell non-autonomous effects together could enhance the differences between the genotypes, with Mecp2+ neurons becoming larger than *Mecp2*$^{+/+}$ to compensate for the smaller Mecp2- neurons. **(F)** Mecp2+ neurons could also be out-competing the smaller Mecp2- neurons, causing Mecp2+ neurons to be larger than *Mecp2*$^{+/+}$ and Mecp2- neurons to be smaller than *Mecp2*$^{-/y}$, indicating both cell autonomous and cell non-autonomous effects.

1.4 Objectives

RTT patients exhibit severe motor abnormalities (Neul et al., 2010), reductions in frontal lobe volume (Reiss et al., 1993) and reduced dendritic arborization of layer V pyramidal neurons in the motor cortex (Belichenko et al., 1994). In view of these findings, our laboratory recently investigated the morphology of pyramidal neurons in the primary motor cortex of *Mecp2*^{Jae} male mice using a yellow fluorescent protein (YFP) transgenic mouse line (Feng et al., 2000) to visualize morphology. It was found that the basal and apical dendritic arbours are reduced in length, and that spine density is reduced on the apical tuft and on oblique apical dendrites (Stuss et al., 2012). The aim of this thesis is to investigate how a mutation in *Mecp2* affects the morphology of the two neuronal genotypes in a female *Mecp2* mutant brain. Due to the interaction between Mecp2 and YFP expression described previously in our lab (Stuss et al., 2012), this thesis visualized the morphology of layer V pyramidal neurons in the primary motor cortex using single cell microinjections of fluorescent dye. Neuronal genotypes were determined after injection using immunohistochemistry in order to separate cell autonomous and cell non-autonomous affects.

It has been proposed the proportion of Mecp2+ and Mecp2- neurons in a RTT female brain affects the phenotype of the patient (Amir et al., 2000) and that these XCI ratios become more skewed over time (Metcalf et al., 2006), however the findings have been inconclusive. Therefore, a goal of this research was to investigate the effects that XCI ratios have on the phenotype of female *Mecp2* mutant mice across age groups, and how XCI ratios affect the robust cellular phenotype markers, soma and nuclear size.

This research indicate that Mecp2- layer V pyramidal neurons in the primary motor cortex of *Mecp2*$^{+/-}$ mice have less total dendritic length triggered by a reduction in the number of third and fourth order branches. Mecp2+ and *Mecp2*$^{+/+}$ were found to be equivalent, suggesting that Mecp2 acts in a cell autonomous manner to affect dendritic length. Interestingly, it was found that the age of mice, observable phenotype and XCI are not correlated. It was also found that the cell autonomous effect of reduced soma and nuclear size of Mecp2- neurons was stable across age groups. However, XCI ratios

correlate with soma and nuclear size of Mecp2- neurons, indicating possible cell non-autonomous competition effects. This data suggests that as the proportion of Mecp2- neurons increases in the brain, the competition from the surrounding neurons decreases, allowing Mecp2- neurons to make more connections, increasing their overall size.

Chapter 2 – Materials and Methods

2.1 Animal Breeding

Heterozygous (*Mecp2*$^{+/-}$) female mice (*Mecp2*$^{tm1.1Jae}$/Mmcd) (MMRRC, UC Davis) (Chen et al., 2001) maintained on a C57BL/6 background and their wild-type littermates (Mecp2$^{+/+}$) were used for soma and nuclear size analysis. Mecp2$^{+/-}$ females were crossed with male YFP-H mice (B6.Cg-Tg(*Thy1-YFP*)HJrs/J) (Feng et al., 2000) homozygous for the transgene on a C57BL/6 background to generate female offspring heterozygous for both *Mecp2* and *YFP-H*. These offspring (*Mecp2*$^{+/-}$/*YFP*$^{+/-}$) and their wild-type littermates (*Mecp2*$^{+/+}$/*YFP*$^{+/-}$) were used for single-cell microinjection experiments. Animal genotypes were determined using PCR (see below). Animals were housed at the University of Victoria Animal Care Unit following approval of protocols by the Animal Care Committee in compliance with the guidelines established by the Canadian Council on Animal Care and Use. Animals were kept at 21° ± 2°C under a 12 hour light/dark cycle with limited environmental enrichment (Lonetti et al., 2010), and given standard laboratory diet and water *ad libitum*.

2.2 Genotyping

Ear clips were obtained from each animal and stored at -20 °C until genomic DNA was extracted using a Qiagen QIAmp DNA Mini Ki (Toronto, ON). PCR was completed using a Biometra T3 Thermocycler (Göttingen, DE). PCR amplification of *Mecp2* sequences was conducted using 1 μl template DNA (250 – 625 ng/μl), 2.5 μl of dNTPs (2mM), 0.25 μl Phusion High Fidelity DNA polymerase (Finnzymes, Vantaa, FI), 5 μl 5X Phusion buffer, 2.5 μl of both forward and reverse primers (10 μM), 3 μl of 60% sucrose/cresol red, and 8.25 μl of ddH_2O. The thermocycler parameters were set as follows: a single denaturation step at 98 °C for 30 seconds, 7 cycles of 10 seconds at 98 °C, 30 seconds at 65 °C decreasing by 1 °C per cycle to 59 °C, and 90 seconds at 72 °C, followed by 23 cycles of 10 seconds at 98 °C, 30 seconds at 58 °C, 90 seconds at 72 °C and finished with a single step at 72 °C for 5 minutes. All samples were held 4 °C until

ready for gel electrophoresis. Primers [5′- CAC CAC AGA AGT ACT ATG ATC -3′] and [5′- ATG CTG ACA AGC TTT CTT CTA -3′] were used to amplify both wild-type (3 kb) or mutant *Mecp2* alleles (250 bp) (Stuss et al., 2012). The *YFP* transgene was amplified using 1 µl template DNA (250 – 625 ng/µl), 2.5 µl of dNTPs (2 mM), 0.25 µl Taq polymerase (Invitrogen, Burlington, ON), 2.5µ 10X PCR buffer, 2.5 µl of forward and reverse primers (10 µM), 3µl of 60% sucrose/cresol red, and 9.75 µl of ddH_2O. The thermocycler parameters were set as follows: a single 150 second denaturation step at 94 °C, 5 cycles of 20 seconds at 94 °C, 30 seconds at 60 °C decreasing by 1 °C per cycle to 56 °C, and 30 seconds at 72 °C, followed by 25 cycles of 20 seconds at 94 °C, 30 seconds at 55 °C, 30 seconds at 72 °C, and finished with a single step at 72 °C for 60 seconds. All samples were held at 4 °C until ready for gel electrophoresis. Primers [5′- TCT GAG TGG CAA AGG ACC TTA GG -3′] and [5′- CGC TGA ACT TGT GGC CGT TTA CG -3′] were used to detect the *YFP* transgene (300 bp). PCR products were run on a 1% (*Mecp2*) or 2% (*YFP*) agarose gel (in 1X TAE) stained with 1X Sybr Safe (Invitrogen). Gels were run with a 1Kb DNA ladder (Invitrogen) visualized using a UVP BioDoc-It-Imaging System UV transilluminator (Upland, CA).

2.3 Perfusion and slice preparation

Before anesthetizing, the phenotype of the mice was scored as described in Table 1. The mice were immobilized with inhalant isofluorane and given an intraperitoneal injection of urethane (0.15 g/ml) (0.3 ml/30 g mouse). Once a mouse was unresponsive to a paw pinch it was pinned down into dorsal recumbency through the forepaws and at the base of the tail. The fur was sprayed with 70% ethanol. A midline abdominal cut was made up to the rib cage, followed by a cut along the bottom of the ribs. The diaphragm was nicked and sliced away from the ribs. The ribs were cut parallel to the sternum up to the apex of the chest. The rib/sternum flap was clamped back with a hemostat to expose the heart. A small cut was made in the right atrium to allow blood to escape. Using a 27 ½ gauge needle on a 10 ml syringe inserted into the tip of the left ventricle, 10 ml of room temperature 0.1 M phosphate buffered saline (PBS) pH 7.4 was used to exsanguinate the mouse (10 ml/min).

Table 1. Phenotype severity scale for the Jaenisch Rett syndrome mouse model (deletion of exon 3 of *Mecp2*)

Parameter	Severity			
Tremors: observed while standing on the palm	No tremor **(0)**	Intermittent mild tremor **(1)**		Continuous tremor or intermittent violent tremor **(2)**
Hind-clasping: observed when suspended by holding the base of the tail	Legs splay outwards **(0)**	Legs are drawn inwards slightly **(1)**	Legs are drawn inwards but do not touch **(2)**	Legs are drawn inward and touch each other and the body tightly **(3)**
Dishevelled fur	Clean and shiny coat **(0)**	Coat dull/ungroomed **(1)**		Piloerection, dull coat/ungroomed **(2)**
Activity level: observed when placed on the bench	WT activity level **(0)**	Slower pace than WT but still active **(1)**	Still for periods, but can move slowly **(2)**	No spontaneous movements **(3)**
Breathing problems	Normal breathing **(0)**	Short periods of rapid breathing or apnea **(1)**		Irregular breathing, gasping or panting **(2)**
Hunched	WT rounded posture **(0)**	Slightly hunched **(1)**		Hunched posture **(2)**

Adapted from Guy et al., (2007).

In mice prepared for single cell microinjections (*YFP*$^{+/-}$: 8 months of age and older) the PBS was followed by perfusion of 30 ml of 4% formaldehyde made from paraformaldehyde (4% PFA) in 0.1 M phosphate buffer pH 6.5 at a rate of 5 ml/min (Berod et al., 1981). The brain was extracted using a dissecting microscope and fine tip forceps, then dropped in 4% PFA pH 6.5 for 10 minutes at room temperature. The brain was removed and placed in a weigh boat.

In mice prepared for soma and nuclear size analysis (5 to 21 months of age), the PBS was followed by perfusion of 10 ml of 4% PFA (pH 6.5, 5 ml/min) and 20 ml of 4% PFA 0.1M borate buffer (pH 11) at a rate of 2 ml/min. The brain was extracted using a dissecting microscope and fine tip forceps, then placed in 4% PFA (pH 11) for two hours at room temperature. The brain was rinsed three times in PBS and immersed in 30% sucrose in PBS containing 0.01% sodium azide at 4 °C for 48 hours.

Brains were prepared for slicing by removing the olfactory bulbs and the cerebellum with a razor blade. The brain was then embedded in 3% agar in 120 mM sodium chloride. The brains were then sliced coronally on a Vibratome Series 1000 (speed 1 amplitude 9, Pelco 101, Redding, CA). The primary motor cortex was identified by the first appearance of the corpus callosum anteriorly and by the joining of the anterior commissure posteriorly. Brains prepared for single cell microinjections ($YFP^{+/-}$) were sliced into approximately ten 200 μm thick sections and then placed in 24 well plates filled with PBS and 0.01% sodium azide and stored at 4 °C until single cell microinjections. Brains prepared for soma and nuclear size analysis were sliced into 50 μm thick sections and then placed in 24 well plates filled with 30% sucrose in PBS and 0.01% sodium azide and stored at 4 °C until immunohistochemistry.

2.4 Single cell microinjections

Slices were placed in a room temperature PBS bath. The cells were visualized using a custom-made epifluorescence microscope equipped with an Olympus UPlanFl 4x/0.13 NA lens (Richmond Hill, ON) and an Olympus LUMPlanFl 40x/0.8 NA water immersion lens. Borosilicate glass pipettes (O.D. 1.5 mm ID 0.86 mm 7.5 cm length fire polished (Sutter Instruments, Novato, CA)) were prepared with a resistance of 5-10MΩ using a micropipette puller (Sutter instruments P-87). Pipettes were dipped in 3 mM Alexa Fluor 594 hydrazide dye (Sigma) and were placed with on a micromanipulator (Narishige) with a silver electrode in contact with the dye. The dye was excited with a 120 W halide arc lamp (EXFO) coupled with a bandpass filter (HQ550/100 M Chroma). Fluorescence was filtered (624/40 Brightline) and subsequently visualized using a CCD camera (Sony) connected to a TV monitor. Layer V was targeted using the YFP+ cells which were faintly visible using the above filter set (Figure 4). Individual neurons were targeted using a translamp and TV monitor with contrast enhancement. Cells were impaled and iontophoretically filled with dye using 3 ms pulses of 3 μA current at 0.5 Hz for 5-10 minutes delivered from a digital stimulator (Neuro Data PG4000) through an isolated current source (Neuro Data SIU90). Neurons were sparsely distributed along the slice (5-10/hemisphere) to ensure that dendrites did not overlap (Figure 4). Cases where the tissue

adhered to the pipette tip were a result of poor fixation and often resulted in dye diffusion out of the cell and/or removal of the nucleus, both leading to rejection of the cell during analysis. Once a slice was complete it was post fixed in 4% PFA pH 11 for 10 minutes at room temperature and then stored in PBS and 0.01% sodium azide at 4 °C.

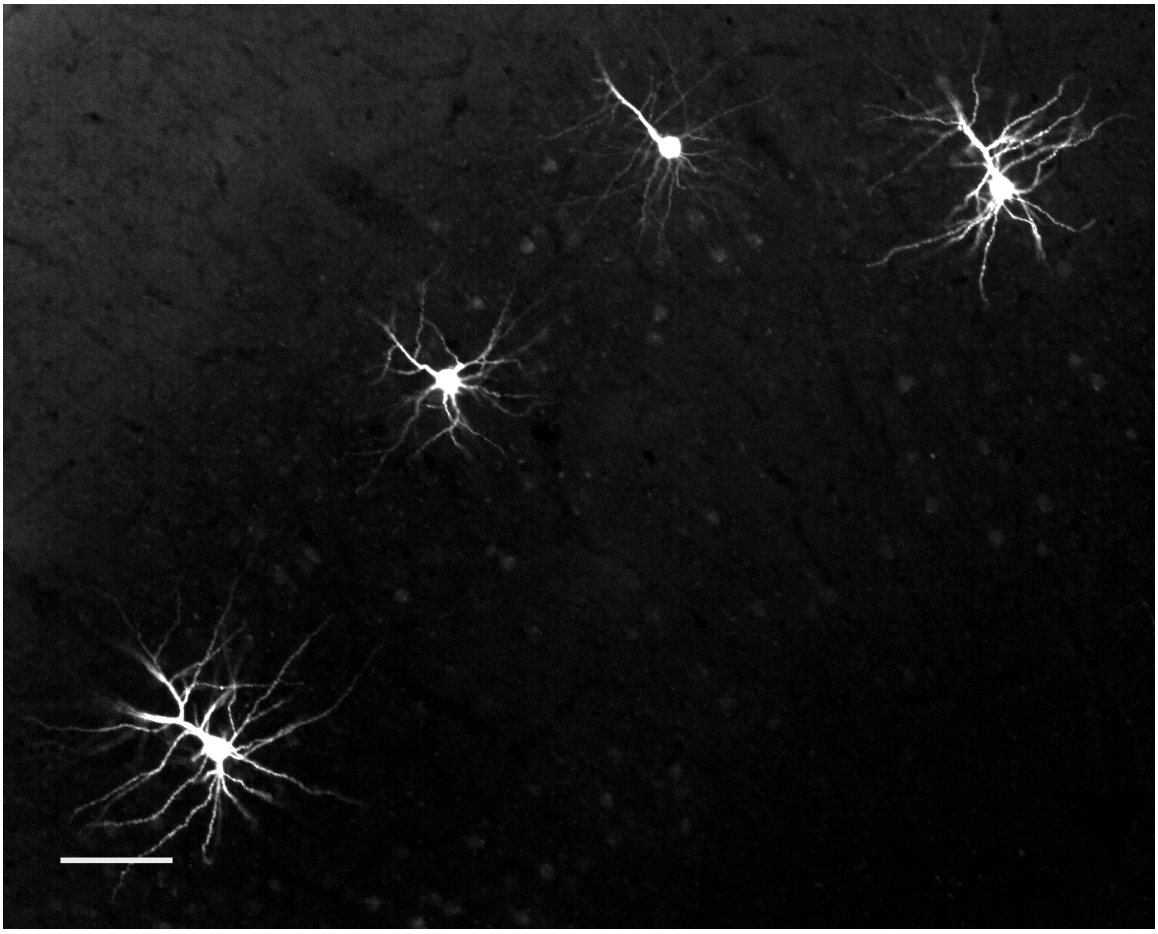

Figure 4. Single cells microinjected with Alexa Fluor 594 dye. Filled neurons were carefully separated across the brain slice in order to maximize the total number of visible cells per slice while preventing overlap of dendrites. YFP-positive neurons faintly label layer V. Scale bar = 100 μm.

2.5 Immunohistochemistry and counterstaining

All immunohistochemistry incubation steps below were performed on floating slices at room temperature on a shaker in the dark with three PBS washes between each step and 0.01% sodium azide added to overnight incubations. All slices were permeabilized with 1% Triton X-100 in PBS for two hours.

Brain slices containing dye filled neurons (*YFP*$^{+/-}$) were immunohistochemically labeled to detect the genotype of individual neurons (Figure 5). Briefly, slices were blocked with 5% normal goat serum in PBS overnight. Slices were then incubated for 24 hours with monoclonal mouse anti-N terminal Mecp2 (binds within the MBD; Sigma 4B6) and monoclonal chicken anti-C terminal Mecp2 (binds end of WW binding region; Millipore ABE171) primary antibodies prepared at 0.2 μg/ml in 1% normal goat serum and PBS. Primary antibodies were detected with goat anti-mouse conjugated to Alexa Fluor 647 (Molecular Probes) and goat anti-chicken conjugated to Alexa Fluor 488 (Molecular Probes) secondary antibodies (4 μg/ml) prepared in 1% normal goat serum and PBS and incubated overnight. Slices were counterstained for 10 minutes with 30 nM of the DNA stain DAPI in PBS.

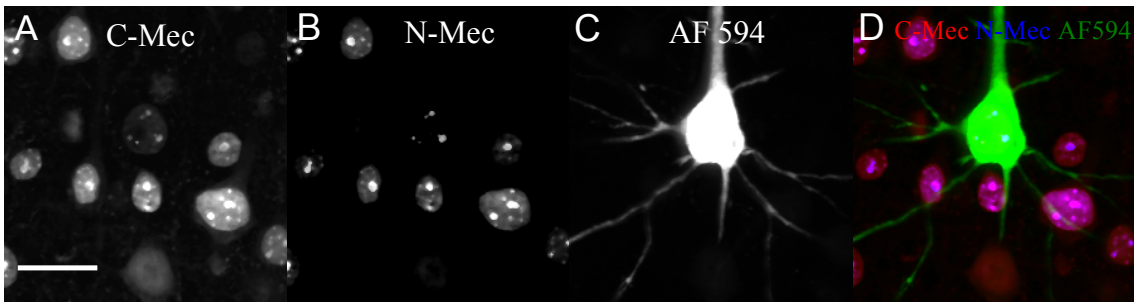

Figure 5. Immunohistochemical genotyping of dye filled neurons. (A) C-terminal Mecp2 antibody (C-Mec) staining appears punctate in Mecp2+ neurons and diffuse in Mecp2- neurons. **(B)** N-terminal Mecp2 (N-Mec) staining appears punctate in Mecp2+ neurons, and is absent in Mecp2- neurons. **(C)** Alexa Fluor 594 (AF 594) fills the cell body and dendrites. **(D)** The composite of all channels reveals the genotype of the desired neuron. Scale bar = 20 μm.

Brain slices prepared for soma and nuclear size analysis (Figure 6) were incubated overnight with monoclonal chicken anti-C terminal Mecp2 (Millipore ABE171) primary antibody prepared at 0.2 μg/ml in PBS. The primary antibody was detected using goat anti-chicken secondary antibodies conjugated to Alexa Fluor 555 (Molecular Probes) prepared at 4 μg/ml in PBS and incubated overnight. Slices were counterstained with DAPI (30 nM) and the deep-red fluorescent Nissl stain Neurotrace 640/660 (Molecular Probes) overnight.

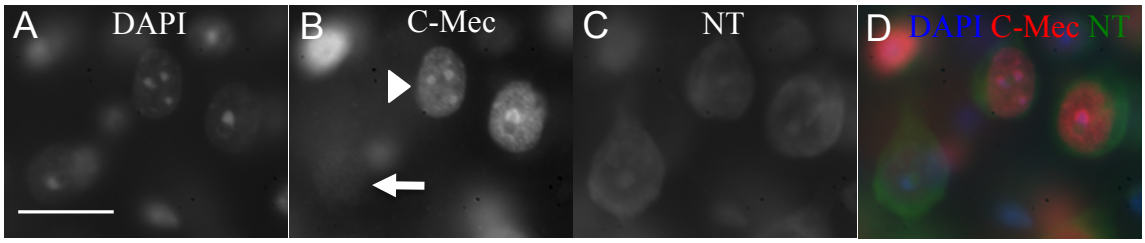

Figure 6. Immunohistochemistry and counterstains for determining soma and nuclear areas. (A) DAPI nuclear labeling reveals whether the cell is the in focal plane and delineates the boundary of nucleus. **(B)** Punctate (arrowhead) or diffuse (arrow) staining of the C-terminal Mecp2 antibody differentiates Mecp2+ and Mecp2- cells respectively. **(C)** The Nissl body stain Neurotrace labels the cytoplasm of neurons. **(D)** Composite reveals the genotype of each neuron. Scale bar = 20 μm.

2.5.1 Lipofuscin reduction

Autofluorescence due to an increase of lipofuscin in older mice interferes with the visibility and quantification of neuronal dendrites (Figure 7B). After the completion of immunohistochemistry and counterstaining protocols lipofuscin fluorescence was quenched by treating cortical slices with 5 mM $CuSO_4$ in 50 mM ammonium acetate for 10 minutes (Figure 7C) (Schnell et al., 1999).

2.5.2 Mounting of brain slices

Slices were mounted on glass slides coated with Poly-L-Lysine (Newcomer Supply) inside a rectangle of Parafilm M (Pechiney Plastic Packaging) that aids in sealing out air around thick (200 μm) sections. Immu-mount (Thermo Scientific) mounting

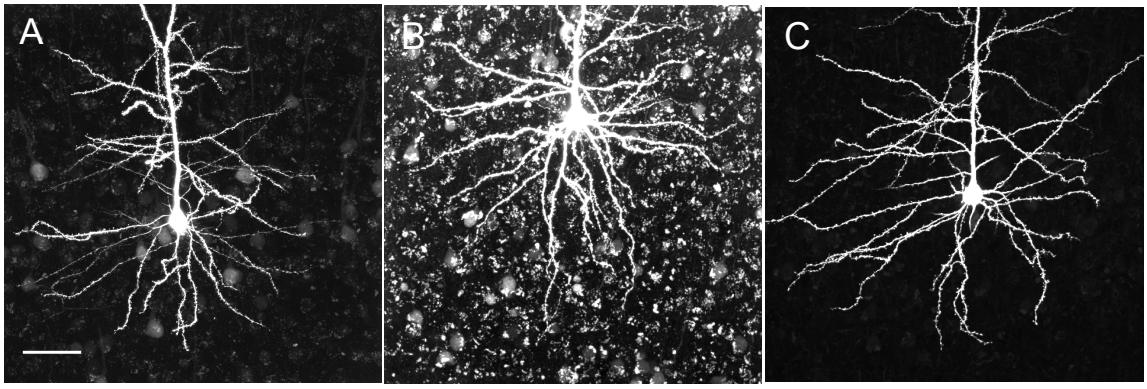

Figure 7. Lipofuscin reduction using $CuSO_4$ treatment. (A) Lipofuscin fluorescence is faint in a brain slice at 9 months of age. **(B)** Lipofuscin increases over time making the visualization and quantification of fluorescent dyes difficult at 18 months. **(C)** When the slices are treated with 5 mM $CuSO_4$ in 50 mM ammonium acetate the lipofuscin fluorescence is drastically reduced. Scale bar = 50 μm.

media was applied and slices were covered with #1.5 glass cover slips (Fisher). Slides were allowed to dry overnight and then were sealed with nail polish. Slides were stored at RT in the dark.

2.6 Fluorescence microscopy

All images for quantification purposes were taken with an Olympus UPlanFL N 40x/1.3 NA oil objective. An Olympus UPlanFl 4x/0.13 NA lens was used to capture images used solely for descriptive purposes (Figure 4). Confocal stacks of single-cells microinjected with Alexa Fluor 594 hydrazide were acquired using a 543 nm laser, 610/100 emission filter, 640 x 640 pixel resolution, 0.5 μm steps, 40 μs/pixel dwell, and high laser power (Figure 7). The high voltage, gain, and offset were modified during imaging to optimize visibility of the dendrites. Any dendrites that ran out of the field of view were captured in a separate adjacent stack. In order to genotype each neuron, a separate confocal stack centered on the cell body at 6x magnification was acquired with additional channels for detection of the C-terminal (488 nm laser, 515/20 filter) and N-terminal (635 nm laser, 705/100 filter) Mecp2 antibodies (Figure 5). All images were exported and saved as tiffs. Brain slices prepared for soma and nuclear size analysis were

viewed on an Olympus IX70 inverted epifluorescence microscope and images (5-10 animal) were captured with a Retiga 2000R digital CCD camera (QImaging, Surrey, BC) with 1.5x zoom, 1600 x 1200 pixel resolution, and minimal gain (Figure 6).

2.7 XCI ratios and soma/nuclear size measurements

Images from 30 *Mecp2*$^{+/-}$ (approximately 45 cells/animal) were analyzed in ImageJ (Abràmoff et al., 2004). Neurons were included if: the nucleus (stained with DAPI) was in the plane of focus, the cell body (labeled with Neurotrace) was not occluded by other cells, and the genotype (C-terminal Mecp2) could be determined. Mecp2+ neurons were counted if DAPI and punctate staining of the C-terminal antibody were visible. Mecp2- neurons were counted if DAPI and diffuse C-terminal antibody staining was visible. Somata (Neurotrace) and nuclei (DAPI) were traced using ImageJ and areas were measured in μm^2.

2.8 Neuronal reconstruction and morphological analysis

This study analyzed 82 *Mecp2*$^{+/+}$ and 157 *Mecp2*$^{+/-}$ (98 Mecp2+, 59 Mecp2-) neurons from five animals per genotype (16-31 cells per animal). When analyzing filled neurons, variation associated with poor fills or chopped dendrites needs to be minimized, therefore neurons were excluded if: 1) the genotype could not be determined, 2) fewer than 3 primary dendrites were intact, 3) more than half of the total primary dendrites on the cell body were chopped off, 4) tips of the dendrites were not visible, or 5) an apical dendrite was not visible. When necessary multiple images stacks were tiled in 3D using the Volume Integration and Alignment System (VIAS) (Rodriguez et al., 2003). ImageJ (Abràmoff et al., 2004) was used to adjust the image brightness/contrast and images were saved as 8-bit tiff files. Three-dimensional neuronal reconstructions were generated in Neuronstudio (Wearne et al., 2005; http://research.mssm.edu/cnic/tools-ns.html) using a Cintiq 21q tablet. Neuron tracings were exported in SWC file format, which is compatible with standard morphometric software tools. Numerous morphological parameters were extracted using freely distributed applications Neuronstudio, Simple

neurite tracer (Longair et al., 2011), and L-Measure (Scorcioni et al., 2008). The morphological measurements chosen for analysis in this study are described in Table 2 and further depicted in Figure 8.

2.9 Statistical Analysis

Statistical analysis was conducted using Prism 5 software (GraphPad). Data are presented as means ± standard error of the mean (SEM). All parameters assessed across Sholl radii or branch orders were analyzed using two-way repeated measures ANOVA with multiple comparisons made using the Bonferroni post-tests. Primary dendrite number was assessed using a one-way ANOVA and multiple comparisons were made using the Bonferroni post-test. Direct comparisons of soma and nuclear areas between genotypes were performed using the non-parametric two-tailed Mann-Whitney test. Linear regressions were used to compare the slopes and y-intercepts of soma and nuclear area data obtained across ages and XCI ratios. Non-linear regressions were fit to the frequency distributions of soma and nuclear areas and the best-fit values were compared. P-values of < 0.05 were considered significant for all statistical tests.

Table 2. Morphological parameters analyzed from 3D neuronal reconstructions

Program	Parameter/Description
Neuronstudio	Total dendritic length (μm)/Sholl radius – Total length of all branches per 10 μm Sholl radius Cumulative dendrite length (μm)/Sholl radius – Cumulative length of all branches totaled at each successive 10 μm Sholl radius Cumulative branch points – Cumulative number of branch points totaled at each successive 10 μm Sholl radius Average branch length per branch order
L-Measure	Number of primary dendrites stemming from the soma Total length of all branches per branch order Number of branch points per branch order Number of branches per branch order Maximum radial distance (μm) - Euclidean distance between the soma and the farthest compartment reached by a dendrite Maximum branch order per 10 μm Sholl radius Path distance per 10 μm Sholl radius Partition asymmetry - $\frac{\lvert T_1 - T_2 \rvert}{T_1 + T_2 - 2}$ where T_1 and T_2 are the number of tips of each daughter tree. Computed at every branch point and plotted as function of branch order

Adapted in part from Scorcioni et al., (2004).

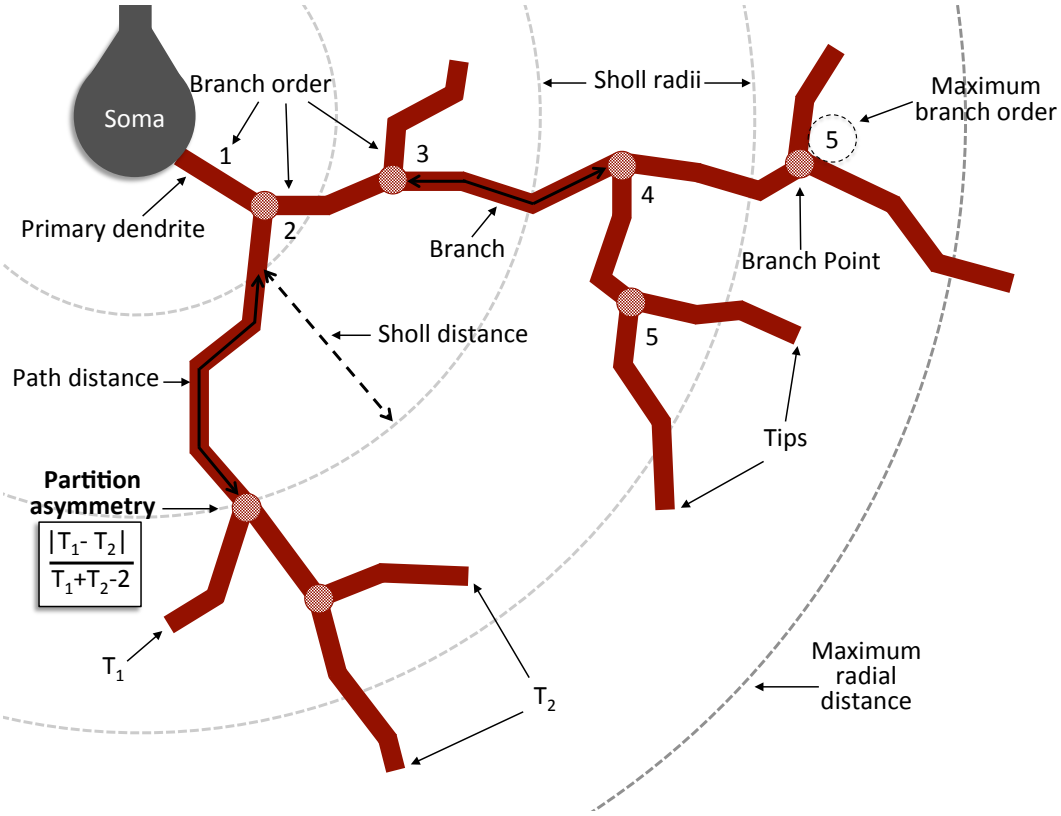

Figure 8. Diagram of morphometric measurements. A *primary dendrite* is any dendrite originating from the cell body. A *branch point* occurs when the original dendrite bifurcates into two or more daughter trees. A centrifugal labeling scheme was used for assigning *branch order*, where the lowest order is given to the primary dendrites and increases when a branch point is reached. *Maximum branch order* is the maximum value reached by any primary tree on a given cell. A *branch* is a length of dendrite between the soma and a branch point, between two branch points, or between a branch point and a tip. A *tip* is the termination of any branch. *Sholl radii* are concentric spheres originating from the centroid of the soma and increasing at 10 μm intervals (Sholl, 1953). *Maximum radial distance* is the maximum Sholl radius reached by any single dendrite per cell. *Path distance* measures the distance along the length of the dendrite, which when plotted against *Sholl distance* depicts the meandering of branches. A slope of 1 would indicate perfectly straight branches, while higher values indicate increased tortuosity. *Partition asymmetry* is calculated at each branch point as $\frac{|T_1 - T_2|}{T_1+T_2-2}$, where T_1 and T_2 are the number of tips of the two daughter trees, with values of one and zero indicating asymmetrical and symmetrical partitioning respectively. Derived in part from Costa et al., (2010).

Chapter 3 – Results

3.1 Morphological analysis of the basal dendritic arbour of layer V pyramidal neurons in the primary motor cortex of *Mecp2*$^{+/+}$ and *Mecp2*$^{+/-}$ mice

3.1.1 Sholl analysis of Mecp2$^{+/+}$, Mecp2+, and Mecp2- neuronal genotypes

Sholl analysis was used to determine how a mutation in *Mecp2* affects the dendritic morphology of Mecp2+ and Mecp2- neurons in relation to Mecp2$^{+/+}$ neurons. The total dendritic length per 10 μm Sholl radius was significantly reduced in Mecp2- neurons 70 to 130 μm from the soma compared to both Mecp2$^{+/+}$ and Mecp2+ genotypes (2-way repeated measures ANOVA and Bonferroni post-tests, $F_{(62,372)} = 2.33$, $p<0.0001$; Figure 9A). Both Mecp2- and Mecp2$^{+/+}$ genotypes peak at 50 μm from the soma (Mecp2- = 168.70 μm ± 7.11, Mecp2$^{+/+}$ = 187.9.27 μm ± 5.14). Mecp2+ neurons peak at 60 μm from the soma (Mecp2+ = 187.29 μm ± 6.17) but Mecp2$^{+/+}$ and Mecp2+ genotypes are not significantly different at any Sholl radius ($p>0.05$) The lines diverge between 30 and 60 μm from the cell body, running parallel after this. This deviation in trend indicates that the subsequent loss of length was initiated in this region and maintained into the distal regions.

Cumulative dendritic length calculated at each successive 10 μm Sholl radius was used (Figure 9B) to determine the total loss of length observed in Figure 9A. Mecp2- neurons have a significant reduction (16% or 298 μm) in cumulative dendritic length compared to the other genotypes, while Mecp2$^{+/+}$ and Mecp2+ are not significantly different (Mecp2- = 1600.57 μm ± 66.20, Mecp2$^{+/+}$ = 1898.54 μm ± 77.64, Mecp2+ = 1873.91 μm ± 66.53; 2-way repeated measures ANOVA and Bonferroni post-tests, $F_{(44,264)} = 4.68$, $p<0.0001$). The maximum radial distance was not significantly different between the genotypes (Mecp2- = 149.7 μm ± 4.29, Mecp2$^{+/+}$ = 159.7 μm ± 5.85, Mecp2+ = 155.5 μm ± 6.15; one-way ANOVA, $F_{(2,12)} = 0.83$, $p=0.5$) suggesting that although Mecp2- neurons are shorter, the reach of their dendritic arbour is unchanged.

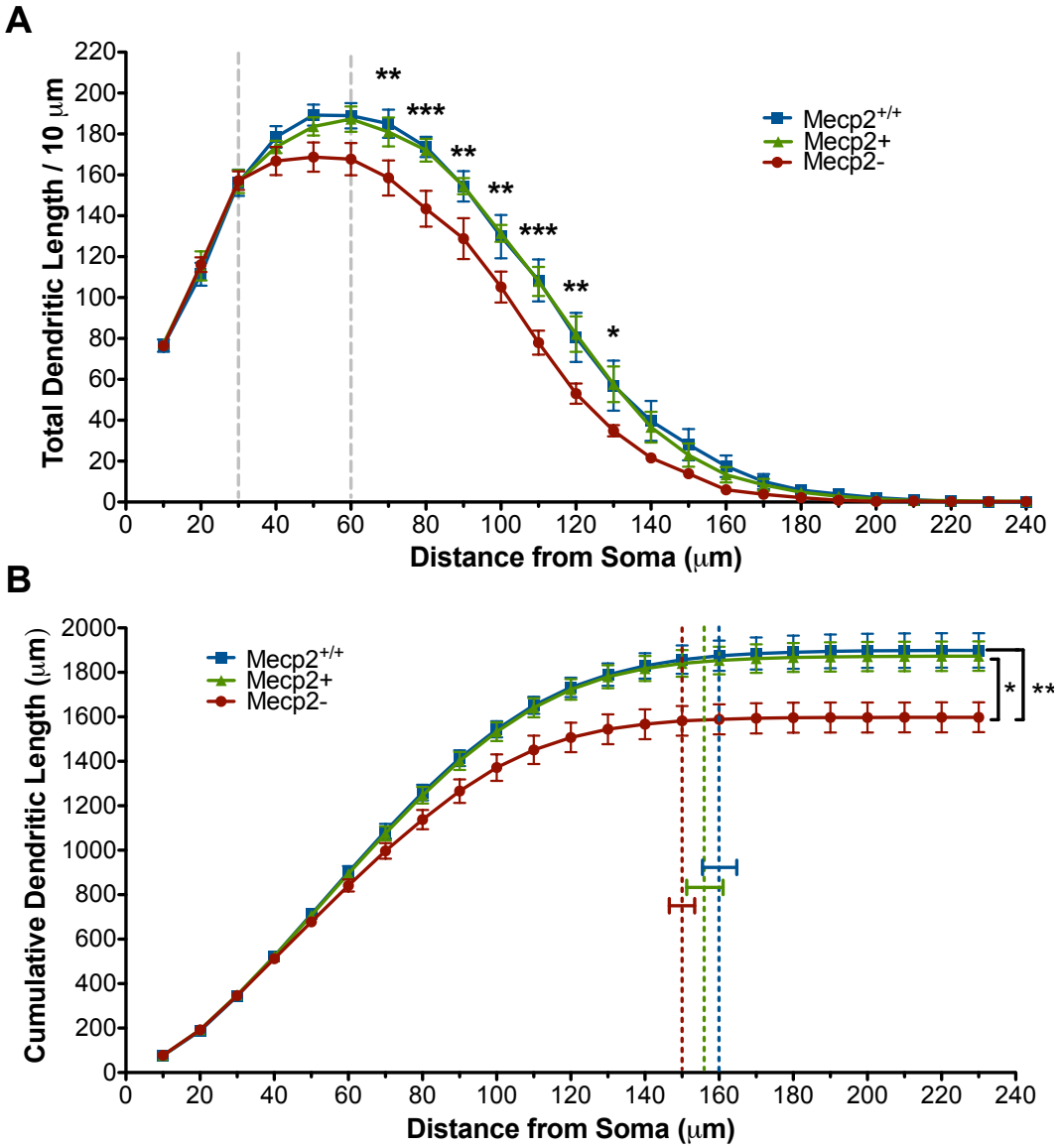

Figure 9. Sholl analysis reveals that Mecp2- neurons have a reduction in total dendritic length. (A) Mecp2- neurons have decreased dendritic length 70 to 130 μm from the soma compared to both Mecp2$^{+/+}$ and Mecp2+ neurons. Dashed lines indicate where the lines diverge. **(B)** Mecp2- neurons total basal dendritic length is significantly reduced by 15% (275 μm) compared to both Mecp2$^{+/+}$ and Mecp2+ neurons. Dashed lines indicate that the average maximum radial distance reached is not significantly different between the genotypes. *p<0.05, **p<0.01, and ***p<0.001.

In order to determine whether Mecp2- neurons have a reduction in length due to a difference in the tortuosity of the branches, branch path distance at each 10 μm Sholl radius was compared (Figure 10A). No statistical differences were found between the genotypes at any Sholl radii (2-way repeated measures ANOVA and Bonferroni post-tests, $F_{(30,180)} = 1.05$, $p=0.4$) indicating the reduction in Mecp2- dendritic length is not due to straighter branches.

The number of primary dendrites was compared (Figure 10B) across neuronal genotypes to determine if Mecp2- neurons have a different number of primary trees that could account for the differences in length observed (Figure 9B). There was no statistical difference in the total number of primary dendrites across all genotypes (one-way ANOVA, $F_{(2,12)} = 0.15$, $p=0.9$).

The number of branch points cumulated at each successive 10 μm Sholl radius (Figure 10C) revealed that Mecp2- neurons have 17% (approximately 3) fewer total branch points than either of the other genotypes (Mecp2- = 13.69 ± 0.70, $Mecp2^{+/+}$ = 16.54 ± 0.43, Mecp2+ = 16.15 ± 0.78; $t_{(24)}=3.51$, $p< 0.01$, 2-way repeated measures ANOVA and Bonferroni post-tests, $F_{(24,144)} = 8.58$, $p<0.0001$). The slopes deviated in trend 30 and 60 μm from the soma suggesting that the branch points were lost in this region.

In order to see if the branch points lost from Mecp2- neurons were from simple (low maximum branch order) or complex (high maximum branch order) primary trees, the maximum branch order reached per cell at each successive 10 μm Sholl radii was compared across the genotypes (Figure 10D). At 60 μm (Mecp2- = 4 ± 0.20, $Mecp2^{+/+}$ = 5 ± 0.25, Mecp2+ = 5 ± 0.20; $t_{(24)}=3.43$, $p<0.05$) and 110 μm (Mecp2- = 4 ± 0.21, $Mecp2^{+/+}$ = 5 ± 0.049, Mecp2+ = 5 ± 0.32; $t_{(24)}=3.43$, $p<0.05$) from the soma, Mecp2- neurons have a significantly lower maximum branch order compared to both other genotypes (2-way repeated measures ANOVA and Bonferroni post-tests, $F_{(2,12)} = 1.381$, $p<0.0001$). This suggests that the branch points are lost from complex branches, thereby reducing the overall dendritic complexity of Mecp2- neurons.

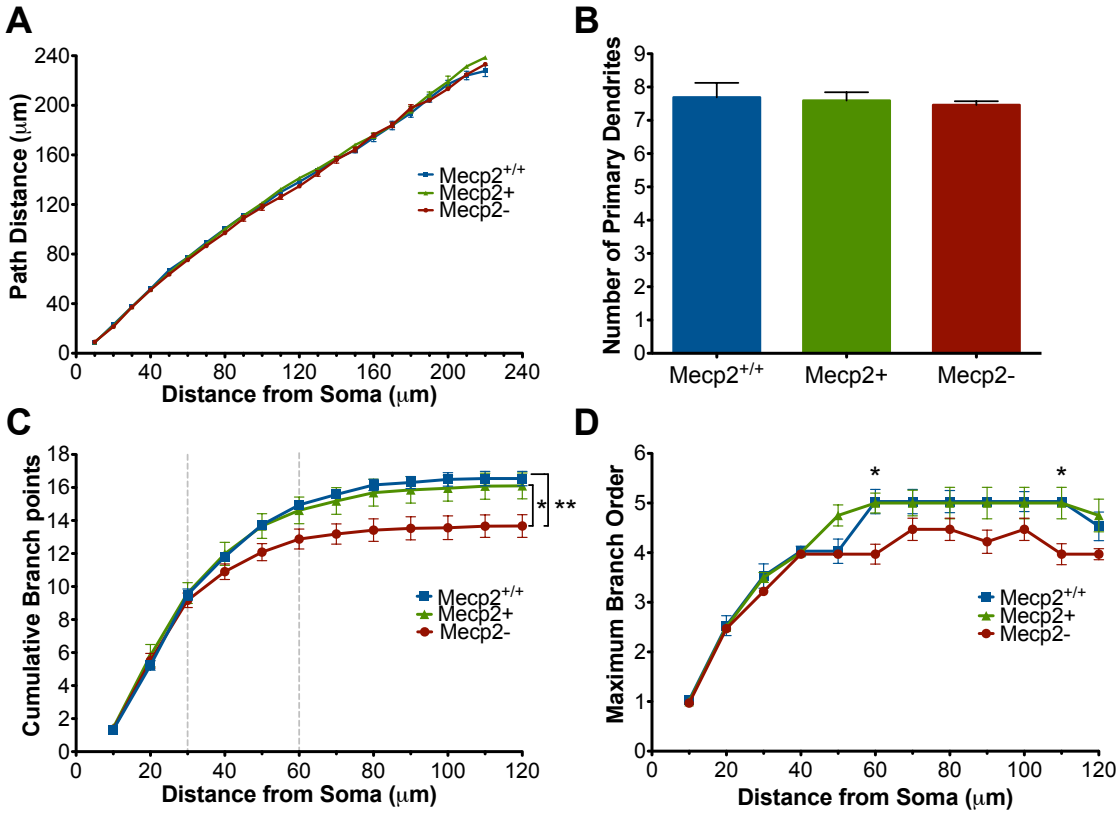

Figure 10. Mecp2- neurons have a reduction in the number of total branch points and maximum branch order reached across Sholl radii. (A) Basal dendrites of all genotypes have similar path distances across Sholl radii. **(B)** All genotypes have the same number of primary dendrites. **(C)** Mecp2- neurons have 17% (approximately 3) fewer total branch points than both other genotypes. Dashed lines indicate where the genotypes deviate in trend. **(D)** The maximum branch order reached by Mecp2- neurons at 60 and 110 μm from the soma is lower than either of the other genotypes. *p<0.05 and **p<0.01.

3.1.2 Branch order analysis of Mecp2$^{+/+}$, Mecp2+, and Mecp2- neurons

Branch order analysis was used to determine how a reduction in total branch point number affects the detailed branch structure of Mecp2- neurons (Figure 11). The number of branch points at each branch order was compared between the neuronal genotypes to see at what level of complexity the branch points were lost (Figure 11B). Mecp2- neurons have fewer branch points at the 2nd (Mecp2- = 4.55 ± 0.29, Mecp2$^{+/+}$ = 5.25 ± 0.13,

Mecp2+ = 5.12 ± 0.38; $t_{(16)}$=3.05, p<0.05) and 3rd (Mecp2- = 2.70 ± 0.19, $Mecp2^{+/+}$ = 3.67 ± 0.31, Mecp2+ = 3.22 ± 0.16; $t_{(16)}$=4.25, p<0.001) branch orders compared to both other genotypes (2-way repeated measures ANOVA and Bonferroni post-tests, $F_{(16,96)}$ = 1.69, p=0.03). Mecp2- neurons therefore have one less branch point at both the second and third branch orders, however this only accounts for two of three lost branch points found (Figure 10C). The remaining branch point is divided across the first and fourth branch orders resulting in insignificant differences between Mecp2- and either of the other neuronal genotypes at these branch orders.

Partition asymmetry was calculated at each branch order to assess whether the branching patterns were altered by the loss of branch points in Mecp2- neurons (Figure 11C). No statistical difference was found between the genotypes across branch orders (2-way repeated measures ANOVA and Bonferroni post-tests, $F_{(8,48)}$ = 2.23 p=0.58) indicating that Mecp2- neurons do not have asymmetrical branching patterns caused by a loss of branch points.

The number of branches per branch order was calculated (Figure 11D) to confirm that the loss of second and third order branch points reduced the number of subsequent branches in the third and fourth branch orders of Mecp2- neurons. It was found that Mecp2- neurons have 16% (approximately 2) fewer 3rd order branches (Mecp2- = 9.21 ± 0.68, $Mecp2^{+/+}$ = 10.98 ± 0.11, Mecp2+ = 10.62 ± 0.67; $t_{(17)}$=3.59, p<0.01) and 25% (approximately 2) fewer 4th order branches (Mecp2- = 5.26 ± 0.31, $Mecp2^{+/+}$ = 6.97 ± 0.66, Mecp2+ = 6.20 ± 0.43; $t_{(14)}$=3.46, p<0.01; 2-way repeated measures ANOVA and Bonferroni post-tests, $F_{(14,84)}$ = 1.51 p=0.02). This data confirms that the loss of second and third order branch points results in the loss of third and fourth order branches.

The total dendritic length per branch order was quantified (Figure 11E) to see if the loss of third and fourth order branches accounted for the total reduction in length observed in Mecp2- neurons. Mecp2- neurons were found to be significantly shorter in the third (17%) and fourth (27%) branch orders as was predicted from the loss of third and fourth order branches (3rd Mecp2- = 499.83 μm ± 28.01, $Mecp2^{+/+}$ = 599.52 μm ±

43.20, Mecp2+ = 554.61 μm ± 50.35; $t_{(14)}$=2.93, p<0.05; 4th Mecp2- = 300.27 μm ± 34.85, Mecp2$^{+/+}$ = 414.01 μm ± 23.91, Mecp2+ = 380.20 μm ± 17.42; $t_{(14)}$=3.34, p<0.01; 2-way repeated measures ANOVA and Bonferroni post-tests, $F_{(14,84)}$ = 1.15 p=0.03). This data indicates that 100 μm of length is lost in third order branches and 115 μm of length is lost at fourth order branches. The remaining unaccounted for reduction in dendritic length (approximately 85 μm) is divided across the second and fifth branch orders.

Finally, the average dendritic length per branch order was assessed (Figure 11F) to determine if a shortening of branches in Mecp2- neurons could account for the reductions in length not attributed to a loss of third and fourth order branches. No statistical difference was found in average branch length per branch order between the genotypes (2-way repeated measures ANOVA and Bonferroni post-tests, $F_{(8,48)}$ = 0.36 p=0.8). This shows that the reduction in dendritic length observed in Mecp2- neurons is not caused from having shorter branches than the other genotypes, but primarily from a loss of third and fourth order branches.

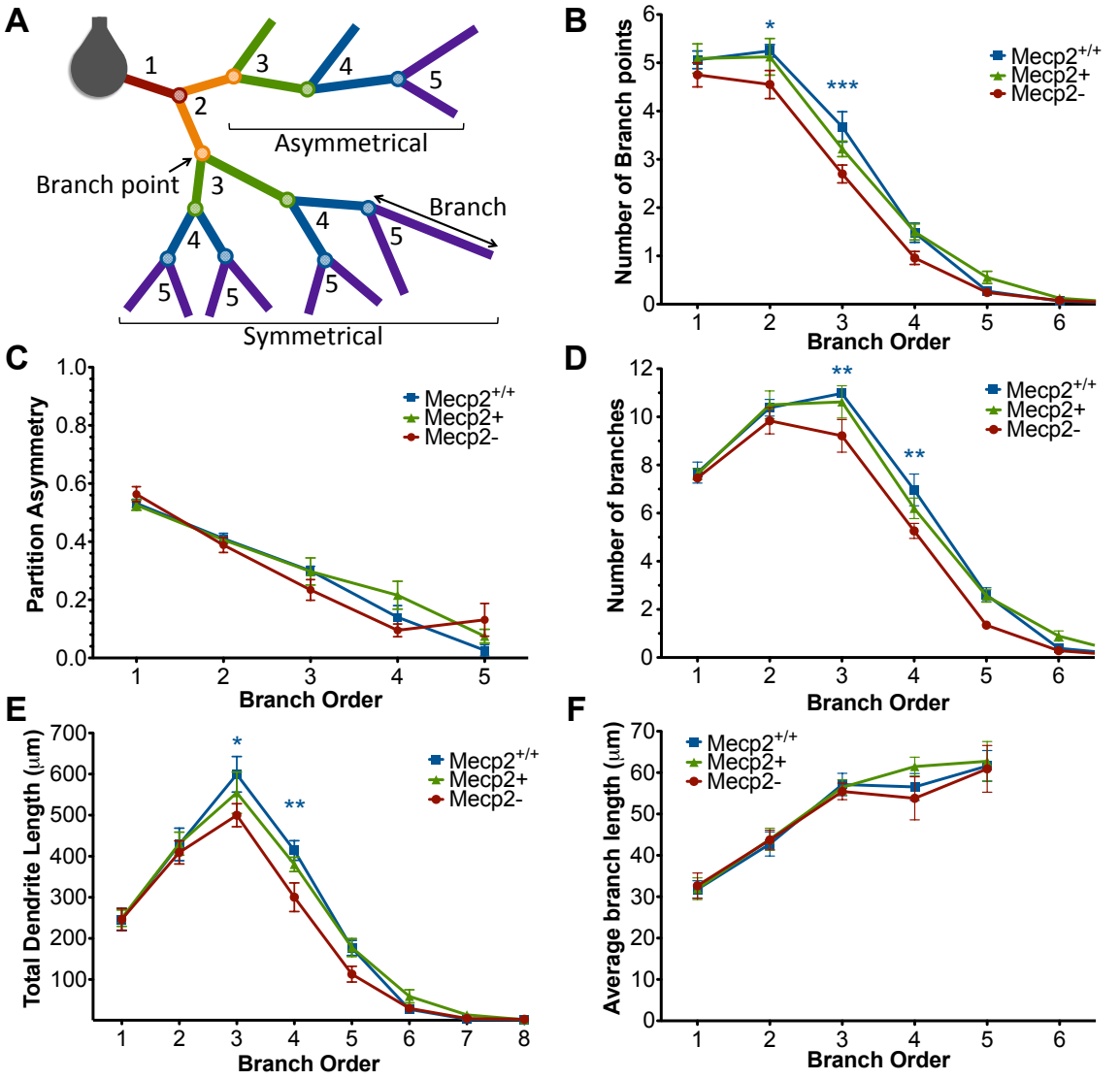

Figure 11. Mecp2- neurons have fewer third and fourth order branches compared to both other genotypes. (A) Branch order diagram depicting the increasing order values with each successive branch point from the cell body. Symmetrical and asymmetrical branching patterns are shown (calculated at the second order branch points) which result in partition asymmetry values of 0 and 1 respectively. **(B)** Mecp2- neurons have fewer second and third order branch points compared to both genotypes. **(C)** Branching patterns in Mecp2- neurons are unaltered. **(D)** Mecp2- neurons have a reduction in dendritic length in the third and fourth branch orders. **(E)** The average length of Mecp2- branches per branch order is unaltered. **(F)** Mecp2- neurons have fewer third and fourth order branches. *p<0.05, **p<0.01 and p<0.001.

3.2 Morphological analysis of soma and nuclear areas of layer V pyramidal neurons in *Mecp2*$^{+/-}$ mice across age and XCI ratios

3.2.1 Analysis of the interaction between age, phenotype, and XCI ratios

To determine the interaction between age, phenotype, and XCI ratios 48 animals were aged to span 2 to 22 months with their phenotype severity recorded at time of death (unless death was premature). The phenotype severity of the animals was highly variable, with mice dying prematurely as young as two months of age, and others surviving into old age (22 months) with only mild symptoms (Figure 12). Premature death occurred in 27% of the population (13 out of 48). Increasing age did not correlate with increased phenotype severity ($p=0.2$, $R^2=0.038$) suggesting that the most severe mice died prematurely or were culled. In order to assess the possibility that XCI ratios were causing the variability in symptom level, XCI ratios were analyzed and compared against phenotype severity. It was found that XCI ratios were not correlated with phenotype severity ($p=0.66$, $R^2=0.0062$). Consequently mice with a highly skewed XCI ratio (10% Mecp2-/90% Mecp2+) favouring expression of the wild-type chromosome did not have less severe symptoms than mice with a more balanced XCI ratio (50% Mecp2-/50% Mecp2+).

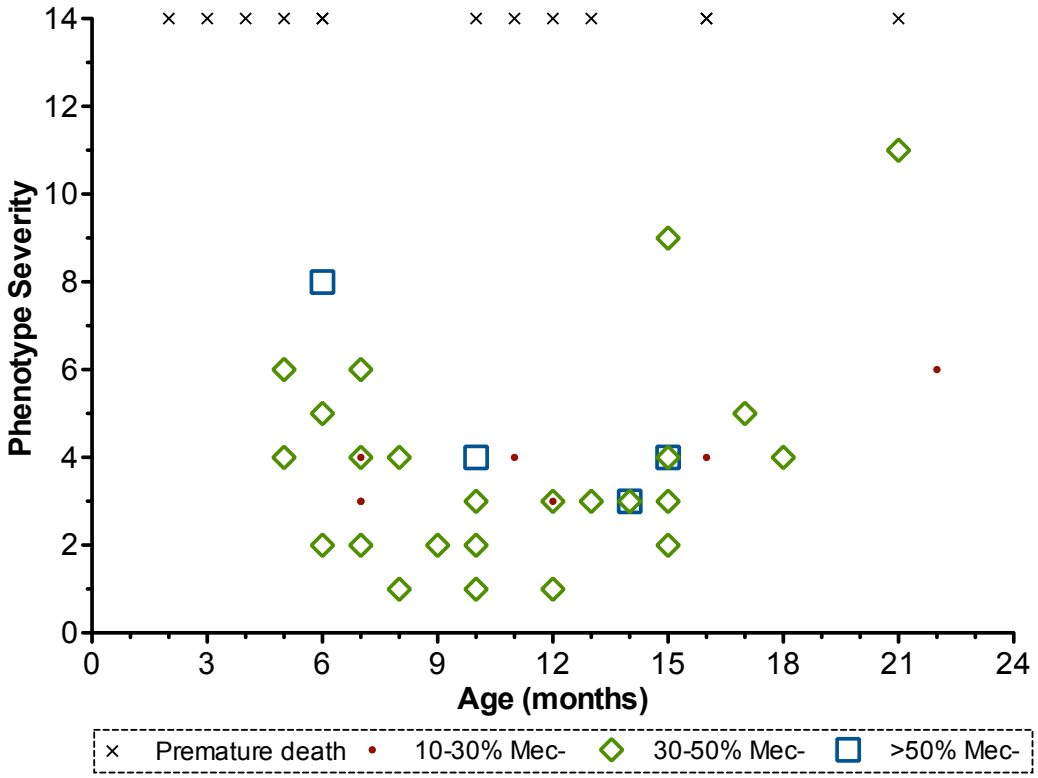

Figure 12. Age, phenotype severity and XCI ratios are not correlated in *Mecp2*$^{+/-}$ mice. Increasing age is not a predictor of phenotype severity of *Mecp2*$^{+/-}$ mice. Aged Mecp2+/-animals are not more likely to have highly skewed XCI ratios (10-30% mutant neurons). XCI ratios do not predict phenotype severity at any age. Premature death occurred across both young and old age groups. Premature death: any animal that died spontaneously, therefore XCI ratios were unavailable, 10-30% Mec-: animals with 10-30% Mecp2- neurons (70-90% Mecp2+ neurons), 30-50% Mec-: animals with 30-50% Mecp2- neurons (50-70% Mecp2+ neurons), >50% Mec-: animals with over 50% Mecp2- neurons (<50% Mecp2+ neurons).

3.2.2 Soma and nuclear area analysis of Mecp2+ and Mecp2- neurons

The nuclear and soma area of Mecp2+ and Mecp2- neuronal genotypes was quantified in layer V pyramidal neurons in the primary motor cortex of *Mecp2*$^{+/-}$ mice (Figure 13). The mean nuclear area of Mecp2- neurons is 14% smaller than Mecp2+ (n=24 animals, Mecp2- = 93.28 μm^2 ± 1.39, Mecp2+ 107.90 μm^2 ± 1.17, $t_{(46)}$=8.04, p<0.0001;Figure 13A). Plotting the population of individual nuclear areas (Mecp2+

n=598 neurons, Mecp2- n=418 neurons, Figure 13B) shows that the smallest nuclei of Mecp2- (52.46 μm^2) and Mecp2+ (58.31 μm^2) genotypes are comparable, while the largest Mecp2- nucleus (174.60 μm^2) is considerably smaller than the largest Mecp2+ nucleus (216.5 μm^2). The mean soma area of Mecp2- neurons is 15% smaller than Mecp2+ (n=24 animals, Mecp2- = 143.3 $\mu m^2 \pm 2.46$, Mecp2+ 169.20 $\mu m^2 \pm 1.94$, $t_{(46)}=8.25$, $p<0.0001$;Figure 13C). The population of individual soma areas (Mecp2+ n=598 neurons, Mecp2- n=418 neurons, Figure 13D) shows that smallest somata of Mecp2- (79.79 μm^2) and Mecp2+ (76.26 μm^2) genotypes are comparable, whereas the largest Mecp2- soma (174.60 μm^2) is considerably smaller than the largest Mecp2+ soma (216.5 μm^2). Frequency distributions of nuclear (Figure 13E) and soma (Figure 13F) areas illustrate how the population of Mecp2- neurons is significantly shifted in comparison to Mecp2+ neurons (nuclear area $t_{(3,21)}=23.66$, $p<0.0001$, soma area $t_{(3,36)}=27.57$, $p<0.0001$). This indicates that the population of Mecp2- neurons has a significant reduction in the number of larger neurons when compared to Mecp2+ neurons, with the smallest neurons of both genotypes being equivalent. Finally, to assess whether the soma or nuclear areas in Mecp2- neurons were reduced disproportionally in relation to each other, the soma and nuclear areas were plotted from Mecp2+ and Mecp2- neurons (Figure 13G). It was found that the slope of Mecp2- and Mecp2+ population trends were not significantly different ($F_{(1,1012)}=1.08$, $p=0.3$) revealing that Mecp2- nuclei are reduced in area proportionately to their soma area when compared to Mecp2+ neurons.

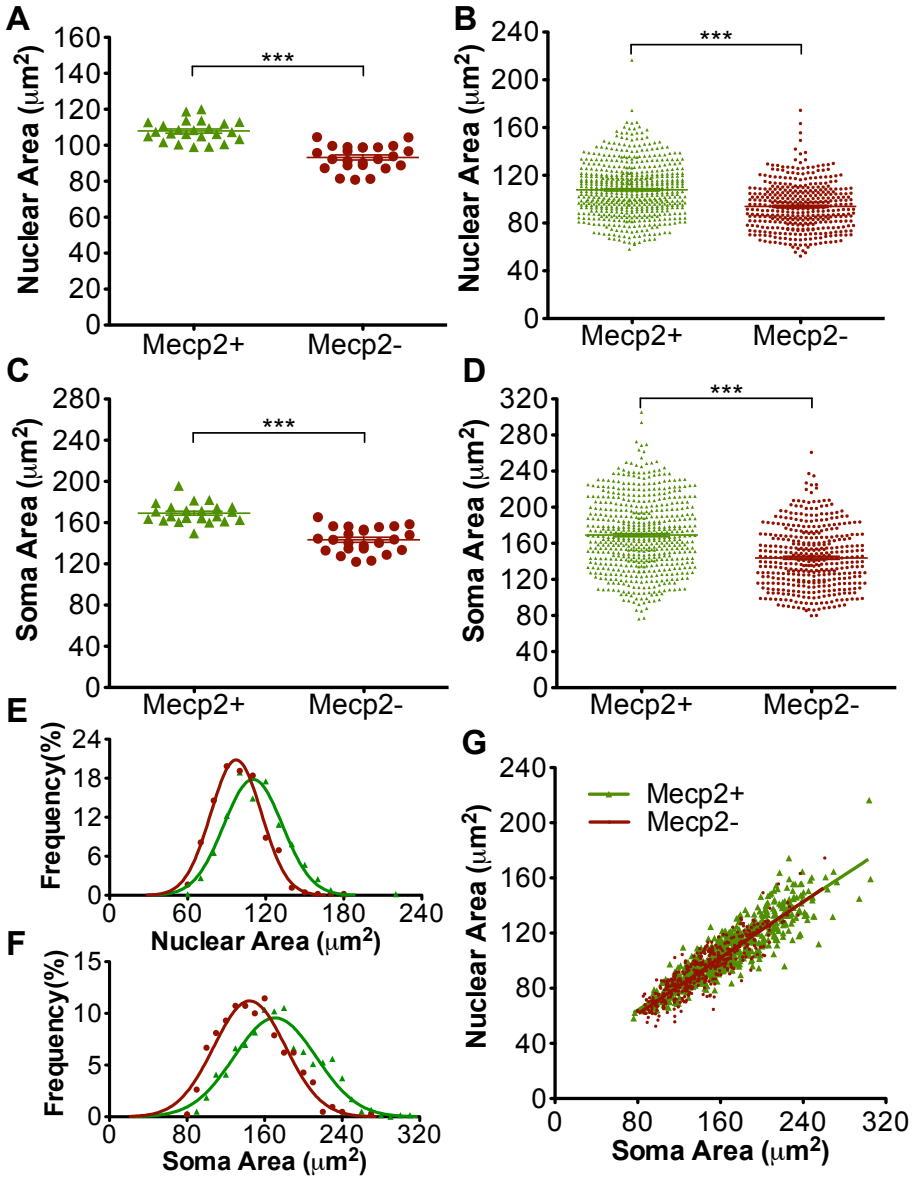

Figure 13. Mecp2- neurons have smaller somata and nuclei than Mecp2+ neurons. Mecp2- nuclei **(A)** and somata **(C)** are on average 13% and 15% smaller than Mecp2+ nuclei and somata, respectively (n=24 animals). The population of individual cells from all animals shows that Mecp2- nuclei **(B)** and somata **(D)** have fewer large nuclei and somata compared to Mecp2+ (Mecp2+ n=598 cells and Mecp2- n=418 cells). Frequency distributions of nuclear **(E)** and somata **(F)** areas are significantly different between the genotypes ($p<0.0001$). Nuclear area Mecp2+ $R^2=0.96$ and Mecp2- $R^2=0.98$. Soma area Mecp2+ $R^2=0.93$ and Mecp2- $R^2=0.94$. **(G)** Soma area is a predictor of nuclear area in both genotypes. Slopes are equal between the genotypes ($p=0.30$). Mecp2+ $R^2=0.79$ and Mecp2- $R^2=0.78$. ***$p<0.001$.

3.2.3 Analysis of the effect of age on soma and nuclear areas

In order to evaluate if age has an effect on the morphology of Mecp2+ and Mecp2- neurons, nuclear and soma areas were plotted against the age of the animal (Figure 14). It was found that age has no effect on the area of nuclei (Mecp2+ $F_{(1,22)}$=0.0089, p=0.92, Mecp2- $F_{(1,22)}$=0.012, p=0.61; Figure 14A) or somata (Mecp2+ $F_{(1,22)}$=0.34, p=0.57, Mecp2- $F_{(1,22)}$=0.069, p=0.79; Figure 14B) of Mecp2+ and Mecp2- neurons. The slope of Mecp2+ and Mecp2- trends are not significantly different in either nuclear ($F_{(1,44)}$=0.21, p=0.65) or soma ($F_{(1,44)}$=0.023, p=0.88) areas plotted across age. This indicates that animals five months and older have comparable nuclear and soma areas in both neuronal genotypes.

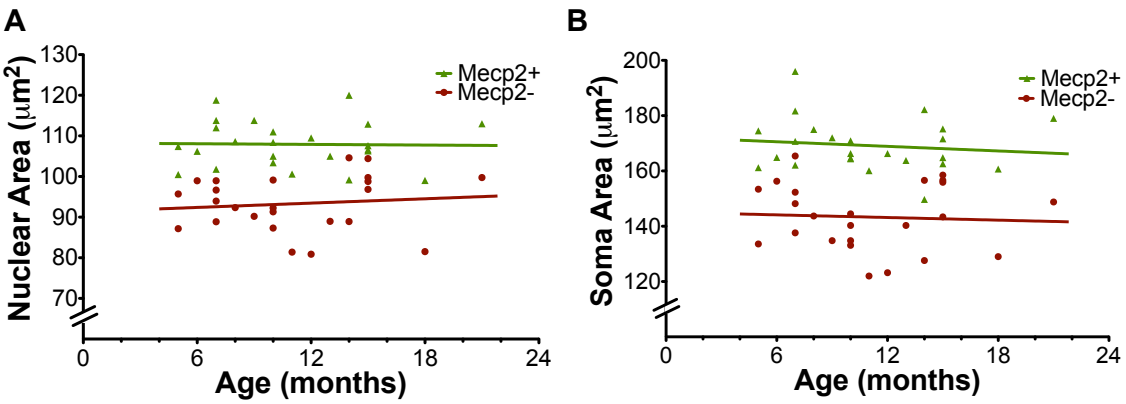

Figure 14. Age does not affect nuclear and soma areas. (A) Nuclear area in Mecp2+ and Mecp2- neurons is not altered across age. Mecp2+ R^2= 0.00040 and Mecp2- R^2=0.012. **(B)** Soma area in both genotypes is not affect by age. Mecp2+ R^2= 0.015 and Mecp2- R^2=0.0031.

3.2.4 Analysis of the effect of XCI ratios on soma and nuclear areas

To determine if XCI ratios have an effect on the morphology of Mecp2+ and Mecp2- neurons, soma and nuclear areas were plotted against the proportion of Mecp2- neurons in the brain (Figure 15). The slope of Mecp2- nuclear area was found to be significantly different from the slope of Mecp2+ nuclear area plotted across the proportion of Mecp2- neurons ($F_{(1,44)}$=4.26, p=0.045; Figure 15A). This indicates that the

nuclear area of Mecp2+ and Mecp2- neurons diverge as the proportion of Mecp2- neurons in the brain decreases. The slope of Mecp2- soma area is not significantly different from Mecp2+ soma area plotted across the proportion of Mecp2- neurons ($F_{(1,44)}$=3.41, p=0.07; Figure 15B), however the trend of divergence of slopes is apparent. In order to minimize for inter-animal differences, Mecp2- areas were normalized to Mecp2+ and plotted across the proportion of Mecp2- neurons in the brain (Figure 15C). The normalized nuclear area of Mecp2- neurons was significantly correlated to the proportion of Mecp2- neurons in the brain ($F_{(1,22)}$=18.14, p=0.0003). The normalized soma area of Mecp2- neurons is significantly correlated to the proportion of Mecp2- neurons in the brain ($F_{(1,22)}$=8.08, p=0.0095). These data suggest that animals with a highly skewed XCI ratio favouring expression of the wild-type allele (<30% Mecp2-/>70% Mecp2+) have the most severe Mecp2- neuronal phenotype (17-22% smaller than Mecp2+). Animals with a balanced XCI ratio (approximately 50% Mecp2-/50% Mecp2+) were found to have Mecp2- neurons with a less severe neuronal phenotype (11-17% smaller than Mecp2+). Therefore as the proportion of Mecp2- neurons in the brain decreases, Mecp2- nuclear and soma areas also decrease.

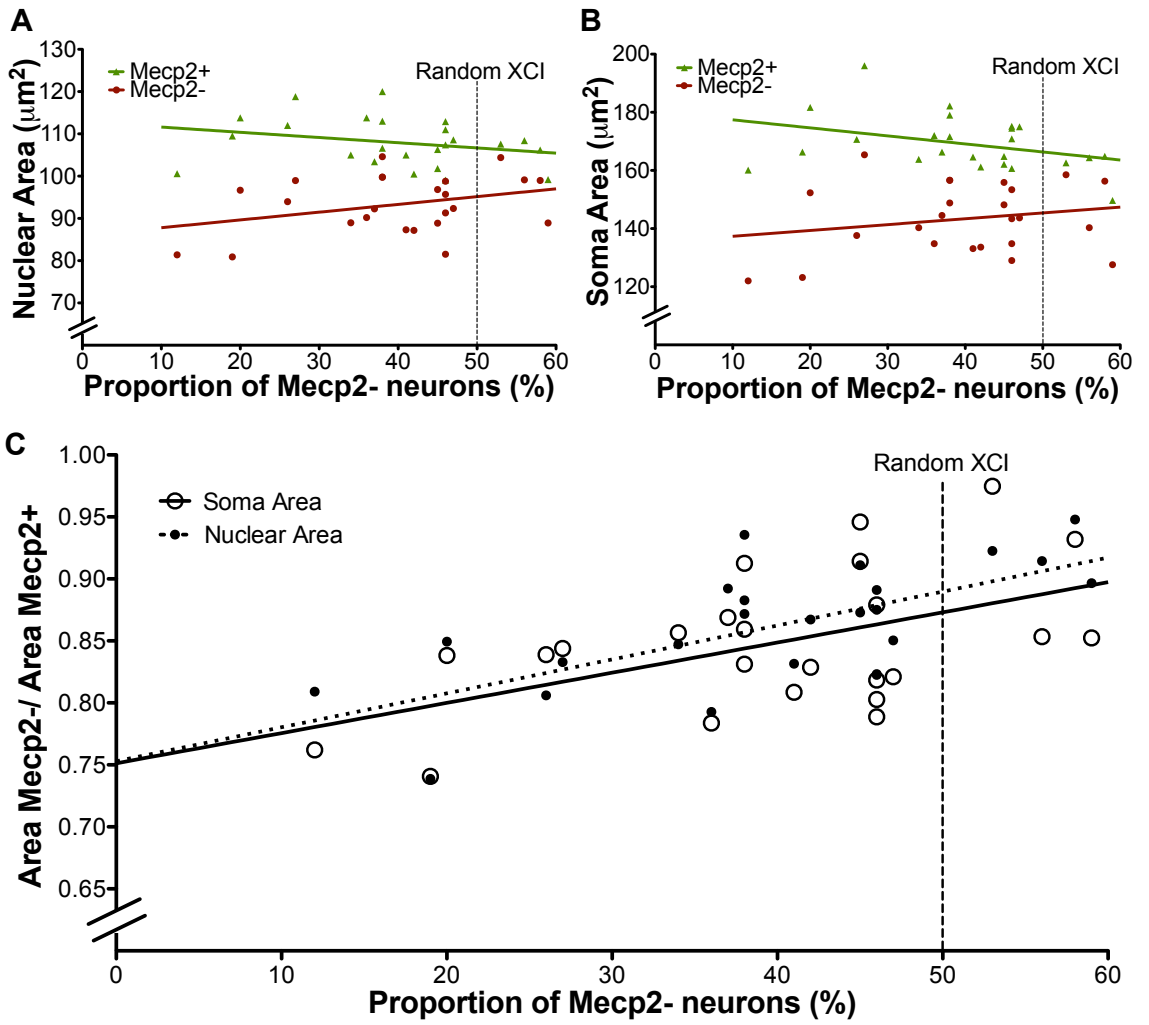

Figure 15. Mecp2- nuclear and soma areas are correlated with XCI ratios.

(A) Nuclear areas of Mecp2+ and Mecp2- neurons diverge as XCI ratios become more skewed favouring expression of Mecp2+ neurons (90% Mecp2+/10% Mecp2-). Slopes are significantly different between the genotypes (p=0.04). Mecp2+ R^2=0.069 and Mecp2- R^2=0.11. **(B)** Soma areas of Mecp2+ and Mecp2- neurons appear to diverge as the proportion of Mecp2- neurons in the brain decreases. Slopes are not significantly different (p=0.07). Mecp2+ R^2=0.13 and Mecp2- R^2=0.041. **(C)** Mecp2- soma and nuclear areas were normalized to Mecp2+ values. Mecp2- nuclei and somata areas at highly skewed XCI ratios (< 30% Mecp2-) are significantly smaller than Mecp2- nuclei and somata areas at more balanced XCI ratios (approximately 50% Mecp2-). Slopes are significantly non-zero (nuclear area p=0.0003 R^2=0.45, soma area p=0.0095 R^2=0.29).

Chapter 4 – Discussion

4.1 Cell autonomous effects of Mecp2 expression on dendritic morphology

4.1.1 Mecp2$^{+/+}$ and Mecp2+ neuronal phenotypes are indistinguishable

This research investigated the consequences of a mutation in *Mecp2* on the morphology of layer V pyramidal neurons in the primary motor cortex of female mice heterozygous for the mutation. The neuronal morphology of Mecp2+ and Mecp2- neurons within the heterozygous female mouse were compared to wild-type female neurons (Mecp2$^{+/+}$). Previous studies have shown Mecp2 deficient glia can cell non-autonomously effect the dendritic morphology of Mecp2+ neurons (Ballas et al., 2009; Lioy et al., 2011). However, the neuronal morphology of Mecp2+ neurons is indistinguishable from Mecp2$^{+/+}$ neurons in all parameters investigated (see Figure 16 for summary), indicating that Mecp2+ neuronal morphology is affected in a cell autonomous manner. These findings may differ from these previous studies due to the proportion of Mecp2 mutant glia in the systems analyzed. The previous research used male mice which have 100% Mecp2 deficient glia, whereas the female mice studied would have varying proportions of Mecp2- glia depending on individual XCI ratios. These findings also differ from other research that found that Mecp2+ layer V pyramidal neurons have fewer basal dendritic spines than Mecp2- and Mecp2$^{+/+}$ neurons, suggesting that Mecp2+ neuronal morphology is affected in a cell non-autonomous manner (Belichenko et al., 2009). The previous study visualized neuronal morphology using a transgenic mouse line expressing green fluorescent protein (GFP) in a subset of neurons (Feng et al., 2000). Mutant *Mecp2* has been found to reduce the expression pattern of YFP in the brain (Stuss et al., 2012), raising the possibility that GFP expression may be silenced in a subset of the population when *Mecp2* is mutated. Therefore, the Mecp2- neurons sampled could be from a subset of the total population, perhaps biasing the analysis. This study was performed by randomly filling layer V neurons with dye, avoiding the possible interactions of endogenous fluorescent protein expression and mutant Mecp2.

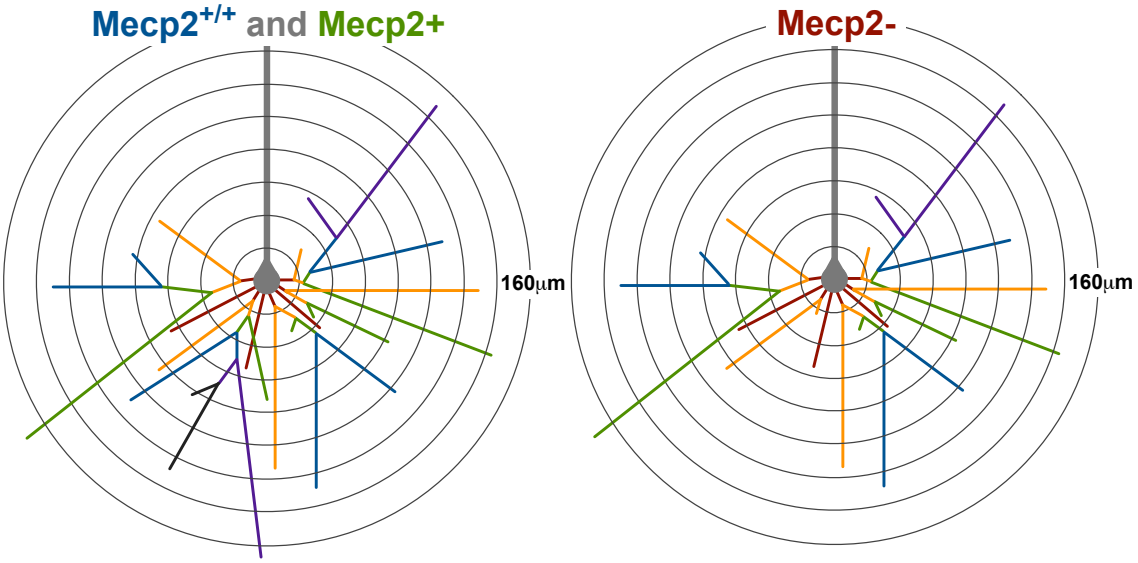

Figure 16. Average Mecp2$^{+/+}$, Mecp2+, and Mecp2- layer V pyramidal neurons. The average Mecp2$^{+/+}$ and Mecp2+ neurons are equivalent across all parameters investigated. The average Mecp2- neuron has approximately 15% less total dendritic length compared to either of the other genotypes. The average Mecp2- neuron has three to four fewer branch points causing a reduction in the number of higher order branches. The maximum branch order is also reduced. Mecp2- neurons have the same average maximum radial distance as both Mecp2$^{+/+}$ and Mecp2+ neurons. Branch order: first = red, second = orange, third = green, fourth = blue, fifth = purple, sixth = black. Radii are 20 μm.

4.1.2 Mecp2- neurons have reductions in total length due to a loss of third and fourth order branches

This research indicates that Mecp2- neurons have a reduction in dendritic length due to a loss of third and fourth order branches (see Figure 16 for summary), which supports previous research in *Mecp2^{Jae}* male mice that found a reduction in the number of higher order branches in layer V pyramidal cells (Stuss et al., 2012). The similar pattern of reduced basal dendritic morphology observed in both Mecp2- and *Mecp2$^{-/y}$* layer V pyramidal neurons indicates that Mecp2 acts in a cell autonomous manner to affect the dendritic morphology of Mecp2- neurons. These results are consistent with other studies that found that Mecp2- callosal projection neurons transplanted into wild-type or *Mecp2$^{-/y}$* brains had primarily cell autonomous reductions in dendritic morphology (Kishi and

Macklis, 2009). Cell autonomous reductions in the dendritic arborization of Mecp2 deficient neurons may be attributed to a decrease in the expression of microtubule-associated protein 2 (MAP-2). RTT patients have lower than normal expression levels of MAP-2 in the brain (Kaufmann et al., 2000). MAP-2 is critical for stabilizing dendritic growth (Kaufmann et al., 1995) and mutations in *MAP-2* have been found to produce RTT-like symptoms in patients (Pescucci et al., 2003).

In contrast with the findings of *Mecp2*$^{-/y}$ neurons in Stuss et al. (2012), the average maximum dendrite radial distance was not reduced in Mecp2- neurons. Additionally, only a 15% reduction in the total dendritic length of Mecp2- neurons was found, whereas a 19% reduction has been previously reported in the layer V pyramidal neurons in *Mecp2*$^{-/y}$ mice (Stuss et al., 2012). This discrepancy between the findings may be due to variation introduced by using different methods of visualizing morphology. Alternatively, the less severe phenotype observed in Mecp2- neurons compared to *Mecp2*$^{-/y}$ neurons may indicate that there are cell non-autonomous effects that may be influencing the morphology of Mecp2- neurons. Mecp2-deficient glia have been found to cell non-autonomously affect dendritic morphology through the release of excess amounts of glutamate (Ballas et al., 2009; Lioy et al., 2011; Maezawa and Jin, 2010; Maezawa et al., 2009; Okabe et al., 2012). Consequently the complete absence of wild-type Mecp2 in the glia of *Mecp2*$^{-/y}$ brains may induce a more severe neuronal phenotype than that observed in *Mecp2*$^{+/-}$ brains where approximately half of the glia express wild-type Mecp2, which may partially alleviate the phenotype of Mecp2- neurons.

In comparison to transgenic mouse lines expressing fluorescent proteins in a subset of neurons in the brain, single cell microinjections enable isolated tracing of single cells thereby increasing the accuracy in determining branching patterns and termination points. However, the single cell microinjections were limited in depth to near the surface of the slice of tissue, consequently filling approximately 50% of the dendritic tree. To ensure that approximately the same proportion of dendritic morphology was intact for quantification, strict guidelines for inclusion were followed (Methods 2.8). These guidelines are effective as all genotypes were found to have the same number of primary

dendrites (Figure 10B). This indicates that Mecp2- neurons did not have a reduction in total dendritic length due to less of the cell being visualized and quantified. Primary trees chopped off at the surface of the slice were included in the analysis, which could have increased the number of lower order branches in all cells. However, in comparison to previous morphological studies of layer V pyramidal neurons (Stuss et al., 2012), there was no increase in the number of lower order branches. In addition, the branching patterns of these filled layer V neurons is consistent with those previously described, as they peak in complexity between 50 and 70 μm from the cell body (Ballesteros-Yáñez et al., 2006). This suggests that this method of morphological visualization does not bias the quantification of dendritic arborization.

4.2 Age, XCI, and animal phenotype are not correlated

Analysis of the observable phenotype of mice at different age groups suggests that in *Mecp2*^{Jae} female mice there is no correlation between the severity of the phenotype and age. This finding is in contrast to previous research that has suggested that certain RTT phenotypes improve as individuals age (Zappella et al., 2003) and that increased age predicts clinical severity (Kaufmann et al., 2011). The most severely affected mice in the population may have succumbed to the their symptoms early in life, while mice with a less severe phenotype could have survived into old age. Therefore it may be misleading to compare these results with longitudinal RTT studies as the phenotype of the mouse was scored only at the time of sacrifice and therefore it is unknown how the severity of the phenotype progressed with time. Interestingly, 27% of the population died prematurely, which is consistent with the rate of sudden death reported in RTT females (26%) (Kerr et al., 1997). Additionally, it was observed that several female mice survived into old age, which has also been reported in RTT females (Hagberg, 2005; Freilinger et al., 2010; Kirby et al., 2010). This suggests that the even though female *Mecp2*^{Jae} mice have a later symptom onset than RTT patients, they may model the advanced stages more accurately than male mice, which die prematurely at 10 weeks (Chen et al., 2001).

It has been suggested that Mecp2- neurons have a survival disadvantage, which may lead to XCI ratios becoming increasingly skewed over time in RTT patients and *Mecp2* mutant mice (Young and Zoghbi, 2004; Smrt et al., 2011; Metcalf et al., 2006). However, these results indicate that older mice are not more likely to have skewed XCI ratios. It cannot be concluded from Young and Zoghbi (2004) that skewed XCI ratios are higher in older female mice, as they found a high rate of skewing in 12 month-old animals but this was not compared to younger age groups. Metcalf et al. (2006) analyzed 20 mice ranging in age from 2 to 24 months, however, this research indicates that a large number of animals should be analyzed in order to observe the less common skewed XCI ratios at any age. Smrt et al. (2011) analyzed the XCI ratios at three, six and nine months of age in 33 mice, however they used an X-linked GFP transgenic mouse line, which has been found in our lab to not label all the expected Mecp2+ neurons (unpublished data), suggesting their assessment of XCI ratios could be inaccurate.

Previous research has suggested that the severity of the RTT phenotype may be influenced by the proportion of Mecp2- neurons in the brain (Young and Zoghbi, 2004; Amir et al., 2000; Weaving et al., 2005; Miltenberger-Miltenyi and Laccone, 2003; Plenge et al., 2002; Sirianni et al., 1998), however this research shows that there is no correlation between XCI ratios in the primary motor cortex and the phenotype severity of the mice. The phenotype was scored without using extensive behavioural tests, which have been shown to reveal subtle abnormalities even in young female mice (Samaco et al., 2012). Because of this, this method may not be an accurate or sensitive measurement of phenotype severity. Additionally, XCI ratios were determined using immunohistochemical analysis of Mecp2+ and Mecp2- neurons in the motor cortex of the brain, whereas other studies use blood or peripheral tissue to determine the XCI ratio, which has been found to not correlate with the XCI in the brain (Gale et al., 1994; Sharp et al., 2000; Young and Zoghbi, 2004).

4.3 Cell autonomous effects on soma and nuclear areas

Reduced soma and nuclear size has become a defining characteristic of RTT since the first morphological studies were performed on post-mortem tissue and on the brains of *Mecp2* mutant mice (Armstrong et al., 1995; Belichenko et al., 1994; Chen et al., 2001). The robust nature of these measurements made them the ideal choice for investigating the perhaps subtle cell non-autonomous effects in a female *Mecp2* mutant brain. However a detailed analysis of soma and nuclear area had not yet been conducted in females while taking into account the two cellular genotypes. These findings are the first detailing how the soma and nuclear areas of Mecp2+ and Mecp2- neurons are affected in a cell autonomous manner in a mosaic female brain.

The analysis of soma areas has revealed that the average Mecp2- soma is smaller than the average Mecp2+ soma confirming previous studies in male *Mecp2*$^{-/y}$ mice (Kishi and Macklis, 2004; Fukuda et al., 2005). When the distribution of individual cells from all animals pooled together was analyzed, it is clear that the Mecp2- population is lacking the largest neurons observed in the Mecp2+ population. The smallest neurons of both genotypes, however, are equivalent. This indicates that mutant Mecp2 may limit the size of neurons, but does not decrease the size of Mecp2- neurons beyond the smallest size of Mecp2+ neurons. It has been shown that smaller somata are correlated with decreased dendritic arborization (Kaufmann et al., 1995), therefore Mecp2 may impact soma size indirectly by regulating the extent of neuronal dendritic arborization.

This research confirms previous studies that have found that Mecp2 controls nuclear size in a cell autonomous manner (Yazdani et al., 2012; Singleton et al., 2011). In the nucleus Mecp2 out competes histone 1 (H1) for bindings sites on DNA (Nikitina et al., 2007; Nan et al., 1997; Ghosh et al., 2010). When Mecp2 is absent or mutated, the levels of H1 in the nucleus double and RNA synthesis is reduced (Yazdani et al., 2012). In addition nucleoli are smaller and more numerous in Mecp2- neurons (Singleton et al., 2011). Elevated levels of H1 cause increased chromatin compaction (Skene et al., 2010), which may result in the reduced nuclear size observed. Mecp2 is required soon after progenitors become post-mitotic, during the rapid growth phase, to regulate neuronal size

and global transcriptional activity (Yazdani et al., 2012). Therefore Mecp2 may act indirectly in the nucleus to regulate its size. Interestingly, soma area was correlated with nuclear area in both cellular genotypes, indicating that neither parameter was reduced to a greater degree than the other in Mecp2- neurons.

4.4 Age does not affect Mecp2+ and Mecp2- neuronal phenotypes

This research has found that soma and nuclear sizes did not correlate with age, which is consistent with previous studies that found that neuronal morphology does not degenerate with increasing age (Armstrong, 1995). As few detectable alterations in gene expression are apparent before symptom onset (Jordan et al., 2007; Kriaucionis et al., 2006; Nuber et al., 2005), it has been proposed that the cellular phenotype may not develop until symptoms are present around six months of age (Guy et al., 2007; Guy et al., 2010). It was found, however, that the cellular phenotype of nearly asymptomatic young mice was not significantly different from severely symptomatic older mice.

4.5 Cell non-autonomous effects of XCI ratios on soma and nuclear areas

This research has shown that as the proportion of Mecp2- neurons in the brain decreases, Mecp2- somata and nuclear sizes also decrease when compared to brains with a higher proportion of Mecp2- neurons. Therefore Mecp2- neurons in female mice with a balanced XCI ratio (approximately 50% Mecp2-) have a less severe cellular phenotype (see Figure 17B for summary) than Mecp2- neurons in females with a highly skewed XCI ratio (see Figure 17C for summary) favoring expression of the wild-type allele (less than 30% Mecp2-). This data suggests that XCI ratios can affect neuronal morphology in a cell non-autonomous manner. Previous research has suggested that a mutation in *Mecp2* may act cell non-autonomously to affect dendritic morphology through the excretion of toxic substances by Mecp2-deficient glia (Ballas et al., 2009; Maezawa et al., 2009; Maezawa and Jin, 2010). This data suggests, however, that this is not a glia mediated cell non-autonomous effect, where higher proportions of Mecp2-deficient glia in the brain would cause deleterious effects on neuronal morphology. It was observed that as the

proportion of Mecp2- neurons in the brain increases, Mecp2- neurons have a less severe phenotype. This indicates that a mutation in *Mecp2* is causing a cell non-autonomous competition effect on the neuronal morphology of Mecp2- layer V pyramidal neurons in addition to the cell autonomous effects discussed above.

These findings are significant, as this pattern of altered competition between the cellular genotypes across XCI ratios has not been previously reported. Given the finding that soma size is correlated with dendritic complexity (Kaufmann et al., 1995), these data suggest that in females with a highly skewed XCI ratio, the surrounding environment is filled with more Mecp2+ neurons that can successfully outcompete Mecp2- neurons for connections. This competition reduces the size of Mecp2- neurons to a greater degree than cell autonomous effects alone. Alternatively in females with a balanced XCI ratio, the environment is less competitive therefore allowing Mecp2- neurons to make more contacts with other surrounding neurons, increasing their overall size.

A cell autonomous reduction in the dendritic morphology of Mecp2- neurons would lead to reduced synaptic activity resulting in less activity dependent phosphorylation of Mecp2 (Buchthal et al., 2012). Serine 421 is present in *Mecp2*^{Jae} mice, therefore activity dependent phosphorylation may impact the function of mutant Mecp2, which has been shown to bind DNA through non-specific interactions with the TRD (Adams et al., 2007). Phosphorylated Mecp2 is normally released from promoters to allow transcription, so a reduction in the activity dependent phosphorylation of Mecp2 would result in less de-repression of target genes needed for synaptic stabilization (Chen et al., 2003). Further research will be needed to fully determine how reduced activity dependent phosphorylation of Mecp2 may cause the cell non-autonomous competition effects that were observed in *Mecp2*$^{+/-}$ mice.

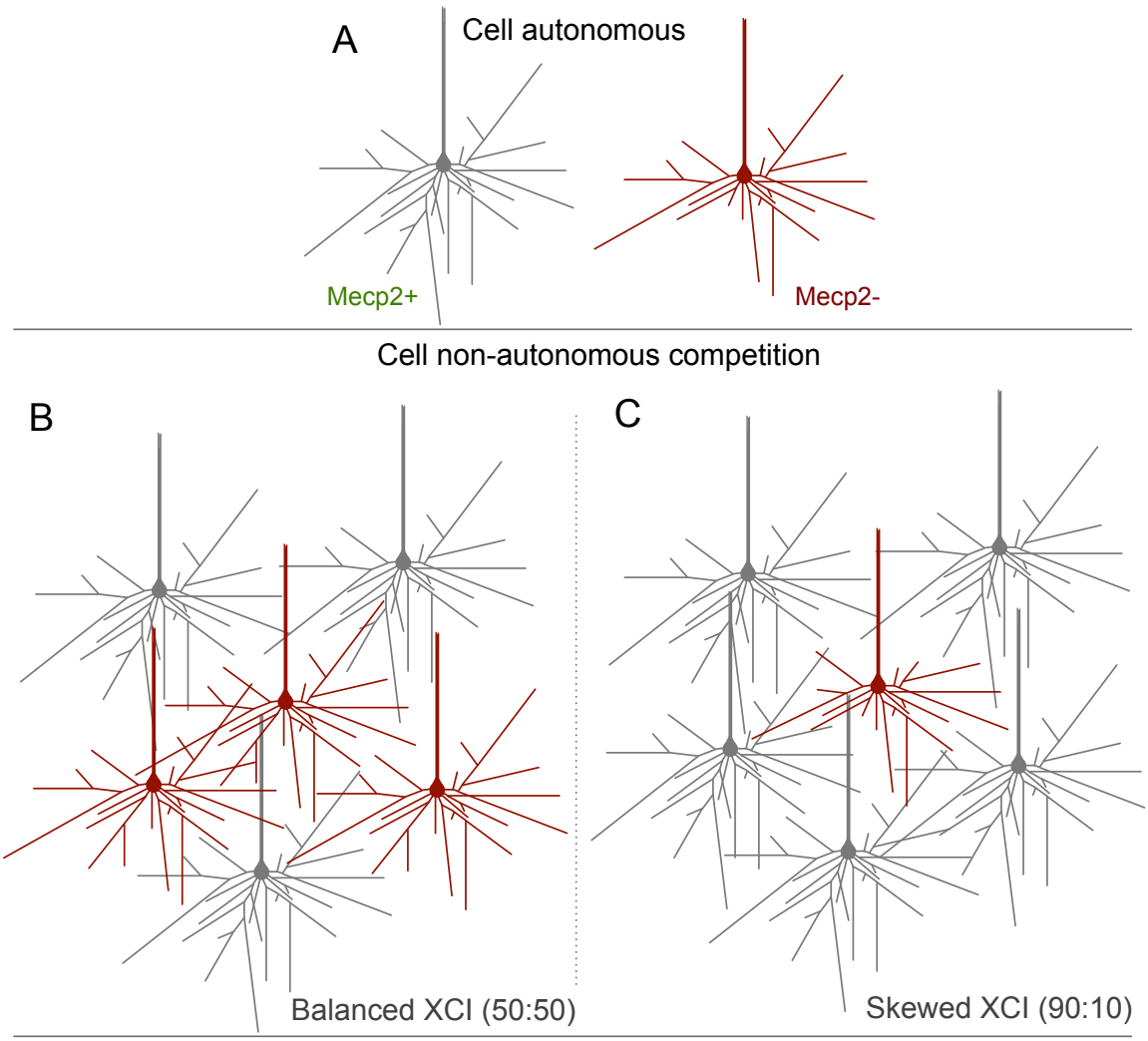

Figure 17. Cell non-autonomous effects of balanced and skewed XCI ratios. (A) Cell autonomous reductions in the morphology of Mecp2- neurons makes them less competitive for synaptic connections. **(B)** A balanced XCI ratio provides Mecp2- neurons more opportunity to make connections as there are fewer large Mecp2+ neurons to compete with. This reduces the severity of the morphological phenotype by up to 10%. **(C)** A skewed XCI ratio favouring Mecp2+ neurons increases the competition for connections. Mecp2- neurons are less able to compete and therefore have a more severe morphological phenotype.

Chapter 5 – Conclusions

This research investigated how a mutation in the X-linked gene *Mecp2* affects layer V pyramidal cell morphology in the primary motor cortex of female *Mecp2*$^{+/-}$ mice. By comparing the two cellular genotypes within *Mecp2*$^{+/-}$ mice (Mecp2+ and Mecp2-) with *Mecp2*$^{+/+}$ neurons it was found that Mecp2$^{+/+}$ neurons and Mecp2+ are indistinguishable, and that Mecp2- neurons have 15% less basal dendritic length than either of the other genotypes due to a 16% reduction in the number of third and fourth order branches. These findings indicate that Mecp2 functions cell autonomously to affect dendritic arborization of layer V pyramidal neurons in *Mecp2*$^{+/-}$ mice.

The effect of age and XCI ratios on the neuronal phenotype in *Mecp2*$^{+/-}$ mice had not been clearly determined in previous research, therefore soma and nuclear areas were analyzed at different ages and XCI ratios to elucidate the interaction. On average, Mecp2- somata are 15% smaller than Mecp2+ and Mecp2- nuclei are13% smaller than Mecp2+. The age of the mouse was found to have no affect on the soma and nuclear area of Mecp2- neurons. The XCI ratio in the brain was found to influence soma and nuclear areas in a cell non-autonomous manner. Female mice with a highly skewed XCI ratio favoring expression of the wild-type allele (less than 30% Mecp2-) have a high proportion of Mecp2+ neurons that can successfully outcompete Mecp2- neurons for connections in the brain, thereby stunting the size of Mecp2- neurons by up to 22% compared to Mecp2+. Female mice with a balanced XCI ratio (approximately 50% Mecp2-) have a higher proportion of Mecp2- neurons than females with a highly skewed XCI ratio. The cell autonomous reduction in size of Mecp2- neurons reduces the surrounding neuronal competition for synaptic connections, therefore allowing Mecp2- neurons to make more contacts with other neurons. This increase in synaptic connectivity results in a 10% increase in size when compared to Mecp2- neurons in a highly skewed environment. This suggests that XCI ratios can affect neuronal morphology in a cell non-autonomous manner.

5.1 Future Directions

This research has shown a novel cell non-autonomous effect of a *Mecp2* mutation on the morphology of layer V pyramidal neurons. The environment surrounding the neurons, consisting of glia and other neurons, can trigger cell non-autonomous effects. It would therefore be necessary to determine whether the XCI ratio quantified in neurons is consistent with that of the surrounding glia. If the XCI ratios are the same between the two cell groups, then the conclusion that the XCI ratio was inducing a cell non-autonomous competition effect on dendritic morphology would be supported. If instead it was determined that the XCI ratio in glia is different from that of neurons, then what was observed may not be competition between neurons, but a more complex deleterious cell non-autonomous glial effect.

Further research is also needed to determine how the reductions in dendritic morphology that was observed affects the physiology of neurons at highly skewed and balanced XCI ratios. Mecp2 deficiency has been found to cause a reduction in inhibitory neurotransmission in the cortex, hippocampus and brain stem, leading to an excess of excitatory neurotransmission (Dani et al., 2005; Medrihan et al., 2008; Zhang et al., 2008). This imbalance of excitatory/inhibitory neurotransmission has been linked to a disruption of long-term potentiation in the hippocampus (Asaka et al., 2006; Weng et al., 2011). Using a transgenic mouse line with GFP-tagged Mecp2 crossed with *Mecp2*^{Jae} mutant mice, it would be possible to approximate the XCI ratio without immunohistochemistry. This would allow quick screening to find animals with rare highly skewed XCI ratios. Additionally, it would be possible to target Mecp2+ and Mecp2- neurons specifically, thereby increasing the number of Mecp2- neurons studied in highly skewed animals. This mouse model could also be used to assess the activity dependent phosphorylation of mutant Mecp2. By performing calcium imaging on Mecp2- neurons, one could determine whether the levels of nuclear calcium are reduced compared to Mecp2+ neurons after synaptic activity (Buchthal et al., 2012).

Bibliography

Abdala, A.P., Dutschmann, M., Bissonnette, J.M., and Paton, J.F. (2010). Correction of respiratory disorders in a mouse model of Rett syndrome. Proc Natl Acad Sci U S A *107*, 18208-213.

Aber, K.M., Nori, P., MacDonald, S.M., Bibat, G., Jarrar, M.H., and Kaufmann, W.E. (2003). Methyl-CpG-binding protein 2 is localized in the postsynaptic compartment: an immunochemical study of subcellular fractions. Neuroscience *116*, 77-80.

Abràmoff, M.D., Magalhães, P.J., and Ram, S.J. (2004). Image processing with ImageJ. Biophotonics international *11*, 36-42.

Adams, V.H., McBryant, S.J., Wade, P.A., Woodcock, C.L., and Hansen, J.C. (2007). Intrinsic disorder and autonomous domain function in the multifunctional nuclear protein, MeCP2. J Biol Chem *282*, 15057-064.

Adler, D.A., Quaderi, N.A., Brown, S.D., Chapman, V.M., Moore, J., Tate, P., and Disteche, C.M. (1995). The X-linked methylated DNA binding protein, Mecp2, is subject to X inactivation in the mouse. Mamm Genome *6*, 491-92.

Ahmed, B., Anderson, J.C., Douglas, R.J., Martin, K.A., and Nelson, J.C. (1994). Polyneuronal innervation of spiny stellate neurons in cat visual cortex. J Comp Neurol *341*, 39-49.

Ahmed, B., Anderson, J.C., Martin, K.A., and Nelson, J.C. (1997). Map of the synapses onto layer 4 basket cells of the primary visual cortex of the cat. J Comp Neurol *380*, 230-242.

Allanson, J.E., Hennekam, R.C., Moog, U., and Smeets, E.E. (2011). Rett syndrome: A study of the face. Am J Med Genet A *155*, 1563-67.

Amir, R.E., and Zoghbi, H.Y. (2000). Rett syndrome: methyl-CpG-binding protein 2 mutations and phenotype-genotype correlations. Am J Med Genet *97*, 147-152.

Amir, R.E., Van den Veyver, I.B., Schultz, R., Malicki, D.M., Tran, C.Q., Dahle, E.J., Philippi, A., Timar, L., Percy, A.K., et al. (2000). Influence of mutation type and X chromosome inactivation on Rett syndrome phenotypes. Ann Neurol *47*, 670-79.

Amir, R.E., Van den Veyver, I.B., Wan, M., Tran, C.Q., Francke, U., and Zoghbi, H.Y. (1999). Rett syndrome is caused by mutations in X-linked MECP2, encoding methyl-CpG-binding protein 2. Nat Genet *23*, 185-88.

Amos-Landgraf, J.M., Cottle, A., Plenge, R.M., Friez, M., Schwartz, C.E., Longshore, J., and Willard, H.F. (2006). X chromosome-inactivation patterns of 1,005 phenotypically unaffected females. Am J Hum Genet *79*, 493-99.

Anderson, J.C., Douglas, R.J., Martin, K.A., and Nelson, J.C. (1994). Synaptic output of physiologically identified spiny stellate neurons in cat visual cortex. J Comp Neurol *341*, 16-24.

Archer, H., Evans, J., Leonard, H., Colvin, L., Ravine, D., Christodoulou, J., Williamson, S., Charman, T., Bailey, M.E., et al. (2007). Correlation between clinical severity in patients with Rett syndrome with a p.R168X or p.T158M MECP2 mutation, and the direction and degree of skewing of X-chromosome inactivation. J Med Genet *44*, 148-152.

Archer, H.L., Whatley, S.D., Evans, J.C., Ravine, D., Huppke, P., Kerr, A., Bunyan, D., Kerr, B., Sweeney, E., et al. (2006). Gross rearrangements of the MECP2 gene are found in both classical and atypical Rett syndrome patients. J Med Genet *43*, 451-56.

Armstrong, D., Dunn, J.K., Antalffy, B., and Trivedi, R. (1995). Selective dendritic alterations in the cortex of Rett syndrome. J Neuropathol Exp Neurol *54*, 195-201.

Armstrong, D.D. (1995). The neuropathology of Rett syndrome--overview 1994. Neuropediatrics *26*, 100-04.

Asaka, Y., Jugloff, D.G., Zhang, L., Eubanks, J.H., and Fitzsimonds, R.M. (2006). Hippocampal synaptic plasticity is impaired in the Mecp2-null mouse model of Rett syndrome. Neurobiol Dis *21*, 217-227.

Babbio, F., Castiglioni, I., Cassina, C., Gariboldi, M.B., Pistore, C., Magnani, E., Badaracco, G., Monti, E., and Bonapace, I.M. (2012). Knock-down of methyl CpG-binding protein 2 (MeCP2) causes alterations in cell proliferation and nuclear lamins expression in mammalian cells. BMC Cell Biol *13*, 19.

Ballas, N., Lioy, D.T., Grunseich, C., and Mandel, G. (2009). Non-cell autonomous influence of MeCP2-deficient glia on neuronal dendritic morphology. Nat Neurosci *12*, 311-17.

Ballesteros-Yáñez, I., Benavides-Piccione, R., Elston, G.N., Yuste, R., and DeFelipe, J. (2006). Density and morphology of dendritic spines in mouse neocortex. Neuroscience *138*, 403-09.

Balmer, D., Goldstine, J., Rao, Y.M., and LaSalle, J.M. (2003). Elevated methyl-CpG-binding protein 2 expression is acquired during postnatal human brain development and is correlated with alternative polyadenylation. J Mol Med *81*, 61-68.

Bannister, A.P. (2005). Inter- and intra-laminar connections of pyramidal cells in the neocortex. Neurosci Res *53*, 95-103.

Bauman, M.L., Kemper, T.L., and Arin, D.M. (1995). Pervasive neuroanatomic abnormalities of the brain in three cases of Rett's syndrome. Neurology *45*, 1581-86.

Belichenko, N.P., Belichenko, P.V., and Mobley, W.C. (2009). Evidence for both neuronal cell autonomous and nonautonomous effects of methyl-CpG-binding protein 2 in the cerebral cortex of female mice with Mecp2 mutation. Neurobiol Dis *34*, 71-77.

Belichenko, N.P., Belichenko, P.V., Li, H.H., Mobley, W.C., and Francke, U. (2008). Comparative study of brain morphology in Mecp2 mutant mouse models of Rett syndrome. J Comp Neurol *508*, 184-195.

Belichenko, P.V., Hagberg, B., and Dahlström, A. (1997). Morphological study of neocortical areas in Rett syndrome. Acta Neuropathol *93*, 50-61.

Belichenko, P.V., Oldfors, A., Hagberg, B., and Dahlström, A. (1994). Rett syndrome: 3-D confocal microscopy of cortical pyramidal dendrites and afferents. Neuroreport *5*, 1509-513.

Belichenko, P.V., Wright, E.E., Belichenko, N.P., Masliah, E., Li, H.H., Mobley, W.C., and Francke, U. (2009). Widespread changes in dendritic and axonal morphology in Mecp2-mutant mouse models of Rett syndrome: evidence for disruption of neuronal networks. J Comp Neurol *514*, 240-258.

Belmont, J.W. (1996). Genetic control of X inactivation and processes leading to X-inactivation skewing. Am J Hum Genet *58*, 1101-08.

Ben-Shachar, S., Chahrour, M., Thaller, C., Shaw, C.A., and Zoghbi, H.Y. (2009). Mouse models of MeCP2 disorders share gene expression changes in the cerebellum and hypothalamus. Hum Mol Genet *18*, 2431-442.

Bermejo-Alvarez, P., Ramos-Ibeas, P., and Gutierrez-Adan, A. (2012). Solving the "X" in embryos and stem cells. Stem Cells Dev *21*, 1215-224.

Berod, A., Hartman, B.K., and Pujol, J.F. (1981). Importance of fixation in immunohistochemistry: use of formaldehyde solutions at variable pH for the localization of tyrosine hydroxylase. J Histochem Cytochem *29*, 844-850.

Bienvenu, T., and Chelly, J. (2006). Molecular genetics of Rett syndrome: when DNA methylation goes unrecognized. Nat Rev Genet *7*, 415-426.

Bissonnette, J.M., and Knopp, S.J. (2006). Separate respiratory phenotypes in methyl-CpG-binding protein 2 (Mecp2) deficient mice. Pediatr Res *59*, 513-18.

Bissonnette, J.M., and Knopp, S.J. (2008). Effect of inspired oxygen on periodic breathing in methy-CpG-binding protein 2 (Mecp2) deficient mice. J Appl Physiol *104*, 198-204.

Bissonnette, J.M., Knopp, S.J., Maylie, J., and Thong, T. (2007). Autonomic cardiovascular control in methyl-CpG-binding protein 2 (Mecp2) deficient mice. Auton Neurosci *136*, 82-89.

Bittel, D.C., Theodoro, M.F., Kibiryeva, N., Fischer, W., Talebizadeh, Z., and Butler, M.G. (2008). Comparison of X-chromosome inactivation patterns in multiple tissues from human females. J Med Genet *45*, 309-313.

Braunschweig, D., Simcox, T., Samaco, R.C., and LaSalle, J.M. (2004). X-Chromosome inactivation ratios affect wild-type MeCP2 expression within mosaic Rett syndrome and Mecp2-/+ mouse brain. Hum Mol Genet *13*, 1275-286.

Brown, C.J., and Robinson, W.P. (2000). The causes and consequences of random and non-random X chromosome inactivation in humans. Clin Genet *58*, 353-363.

Buchthal, B., Lau, D., Weiss, U., Weislogel, J.M., and Bading, H. (2012). Nuclear Calcium Signaling Controls Methyl-CpG-binding Protein 2 (MeCP2) Phosphorylation on Serine 421 following Synaptic Activity. J Biol Chem *287*, 30967-974.

Burkhalter, A., and Bernardo, K.L. (1989). Organization of corticocortical connections in human visual cortex. Proc Natl Acad Sci U S A *86*, 1071-75.

Buschdorf, J.P., and Strätling, W.H. (2004). A WW domain binding region in methyl-CpG-binding protein MeCP2: impact on Rett syndrome. J Mol Med *82*, 135-143.

Campos, M., Churchman, S.M., Santos-Rebouças, C.B., Ponchel, F., and Pimentel, M.M. (2010). High frequency of nonrecurrent MECP2 duplications among Brazilian males with mental retardation. J Mol Neurosci *41*, 105-09.

Carrel, L., and Willard, H.F. (2005). X-inactivation profile reveals extensive variability in X-linked gene expression in females. Nature *434*, 400-04.

Carter, J.C., Lanham, D.C., Pham, D., Bibat, G., Naidu, S., and Kaufmann, W.E. (2008). Selective cerebral volume reduction in Rett syndrome: a multiple-approach MR imaging study. AJNR Am J Neuroradiol *29*, 436-441.

Casanova, M.F., Naidu, S., Goldberg, T.E., Moser, H.W., Khoromi, S., Kumar, A., Kleinman, J.E., and Weinberger, D.R. (1991). Quantitative magnetic resonance imaging in Rett syndrome. J Neuropsychiatry Clin Neurosci *3*, 66-72.

Chae, J.H., Hwang, H., Hwang, Y.S., Cheong, H.J., and Kim, K.J. (2004). Influence of MECP2 gene mutation and X-chromosome inactivation on the Rett syndrome phenotype. J Child Neurol *19*, 503-08.

Chahrour, M., Jung, S.Y., Shaw, C., Zhou, X., Wong, S.T., Qin, J., and Zoghbi, H.Y. (2008). MeCP2, a key contributor to neurological disease, activates and represses transcription. Science *320*, 1224-29.

Chandler, S.P., Guschin, D., Landsberger, N., and Wolffe, A.P. (1999). The methyl-CpG binding transcriptional repressor MeCP2 stably associates with nucleosomal DNA. Biochemistry *38*, 7008-018.

Chao, H.T., Chen, H., Samaco, R.C., Xue, M., Chahrour, M., Yoo, J., Neul, J.L., Gong, S., Lu, H.C., et al. (2010). Dysfunction in GABA signalling mediates autism-like stereotypies and Rett syndrome phenotypes. Nature *468*, 263-69.

Chapleau, C.A., Boggio, E.M., Calfa, G., Percy, A.K., Giustetto, M., and Pozzo-Miller, L. (2012). Hippocampal CA1 Pyramidal Neurons of Mecp2 Mutant Mice Show a Dendritic Spine Phenotype Only in the Presymptomatic Stage. Neural Plast *2012*, 976164.

Chapleau, C.A., Calfa, G.D., Lane, M.C., Albertson, A.J., Larimore, J.L., Kudo, S., Armstrong, D.L., Percy, A.K., and Pozzo-Miller, L. (2009). Dendritic spine pathologies in hippocampal pyramidal neurons from Rett syndrome brain and after expression of Rett-associated MECP2 mutations. Neurobiol Dis *35*, 219-233.

Charman, T., Neilson, T.C., Mash, V., Archer, H., Gardiner, M.T., Knudsen, G.P., McDonnell, A., Perry, J., Whatley, S.D., et al. (2005). Dimensional phenotypic analysis and functional categorisation of mutations reveal novel genotype-phenotype associations in Rett syndrome. Eur J Hum Genet *13*, 1121-130.

Chen, R.Z., Akbarian, S., Tudor, M., and Jaenisch, R. (2001). Deficiency of methyl-CpG binding protein-2 in CNS neurons results in a Rett-like phenotype in mice. Nat Genet *27*, 327-331.

Chen, W.G., Chang, Q., Lin, Y., Meissner, A., West, A.E., Griffith, E.C., Jaenisch, R., and Greenberg, M.E. (2003). Derepression of BDNF transcription involves calcium-dependent phosphorylation of MeCP2. Science *302*, 885-89.

Cheval, H., Guy, J., Merusi, C., De Sousa, D., Selfridge, J., and Bird, A. (2012). Postnatal inactivation reveals enhanced requirement for MeCP2 at distinct age windows. Hum Mol Genet *21*, 3806-814.

Cohen, S., Gabel, H.W., Hemberg, M., Hutchinson, A.N., Sadacca, L.A., Ebert, D.H., Harmin, D.A., Greenberg, R.S., Verdine, V.K., et al. (2011). Genome-wide activity-

dependent MeCP2 phosphorylation regulates nervous system development and function. Neuron *72*, 72-85.

Collins, A.L., Levenson, J.M., Vilaythong, A.P., Richman, R., Armstrong, D.L., Noebels, J.L., David Sweatt, J., and Zoghbi, H.Y. (2004). Mild overexpression of MeCP2 causes a progressive neurological disorder in mice. Hum Mol Genet *13*, 2679-689.

Costa, L.d.a. .F., Zawadzki, K., Miazaki, M., Viana, M.P., and Taraskin, S.N. (2010). Unveiling the neuromorphological space. Front Comput Neurosci *4*, 150.

Dani, V.S., Chang, Q., Maffei, A., Turrigiano, G.G., Jaenisch, R., and Nelson, S.B. (2005). Reduced cortical activity due to a shift in the balance between excitation and inhibition in a mouse model of Rett syndrome. Proc Natl Acad Sci U S A *102*, 12560-65.

Derecki, N.C., Cronk, J.C., Lu, Z., Xu, E., Abbott, S.B., Guyenet, P.G., and Kipnis, J. (2012). Wild-type microglia arrest pathology in a mouse model of Rett syndrome. Nature *484*, 105-09.

Dragich, J.M., Kim, Y.H., Arnold, A.P., and Schanen, N.C. (2007). Differential distribution of the MeCP2 splice variants in the postnatal mouse brain. J Comp Neurol *501*, 526-542.

Feng, G., Mellor, R.H., Bernstein, M., Keller-Peck, C., Nguyen, Q.T., Wallace, M., Nerbonne, J.M., Lichtman, J.W., and Sanes, J.R. (2000). Imaging neuronal subsets in transgenic mice expressing multiple spectral variants of GFP. Neuron *28*, 41-51.

Freilinger, M., Bebbington, A., Lanator, I., De Klerk, N., Dunkler, D., Seidl, R., Leonard, H., and Ronen, G.M. (2010). Survival with Rett syndrome: comparing Rett's original sample with data from the Australian Rett Syndrome Database. Dev Med Child Neurol *52*, 962-65.

Fukuda, T., Itoh, M., Ichikawa, T., Washiyama, K., and Goto, Y. (2005). Delayed maturation of neuronal architecture and synaptogenesis in cerebral cortex of Mecp2-deficient mice. J Neuropathol Exp Neurol *64*, 537-544.

Fyffe, S.L., Neul, J.L., Samaco, R.C., Chao, H.T., Ben-Shachar, S., Moretti, P., McGill, B.E., Goulding, E.H., Sullivan, E., et al. (2008). Deletion of Mecp2 in Sim1-expressing neurons reveals a critical role for MeCP2 in feeding behavior, aggression, and the response to stress. Neuron *59*, 947-958.

Gale, R.E., Wheadon, H., Boulos, P., and Linch, D.C. (1994). Tissue specificity of X-chromosome inactivation patterns. Blood *83*, 2899-2905.

Gantz, S.C., Ford, C.P., Neve, K.A., and Williams, J.T. (2011). Loss of mecp2 in substantia nigra dopamine neurons compromises the nigrostriatal pathway. J Neurosci *31*, 12629-637.

Georgel, P.T., Horowitz-Scherer, R.A., Adkins, N., Woodcock, C.L., Wade, P.A., and Hansen, J.C. (2003). Chromatin compaction by human MeCP2. Assembly of novel secondary chromatin structures in the absence of DNA methylation. J Biol Chem *278*, 32181-88.

Ghosh, R.P., Horowitz-Scherer, R.A., Nikitina, T., Shlyakhtenko, L.S., and Woodcock, C.L. (2010). MeCP2 binds cooperatively to its substrate and competes with histone H1 for chromatin binding sites. Mol Cell Biol *30*, 4656-670.

Gilbert, C.D. (1993). Circuitry, architecture, and functional dynamics of visual cortex. Cereb Cortex *3*, 373-386.

Guy, J., Cheval, H., Selfridge, J., and Bird, A. (2010). The Role of MeCP2 in the Brain. Annu Rev Cell Dev Biol *27*, 631-652.

Guy, J., Gan, J., Selfridge, J., Cobb, S., and Bird, A. (2007). Reversal of neurological defects in a mouse model of Rett syndrome. Science *315*, 1143-47.

Guy, J., Hendrich, B., Holmes, M., Martin, J.E., and Bird, A. (2001). A mouse Mecp2-null mutation causes neurological symptoms that mimic Rett syndrome. Nat Genet *27*, 322-26.

Hagberg, B. (2005). Rett syndrome: long-term clinical follow-up experiences over four decades. J Child Neurol *20*, 722-27.

Horike, S., Cai, S., Miyano, M., Cheng, J.F., and Kohwi-Shigematsu, T. (2005). Loss of silent-chromatin looping and impaired imprinting of DLX5 in Rett syndrome. Nat Genet *37*, 31-40.

Ishii, T., Makita, Y., Ogawa, A., Amamiya, S., Yamamoto, M., Miyamoto, A., and Oki, J. (2001). The role of different X-inactivation pattern on the variable clinical phenotype with Rett syndrome. Brain Dev *23 Suppl 1*, S161-64.

Jellinger, K., and Seitelberger, F. (1986). Neuropathology of Rett syndrome. Am J Med Genet Suppl *1*, 259-288.

Jellinger, K., Armstrong, D., Zoghbi, H.Y., and Percy, A.K. (1988). Neuropathology of Rett syndrome. Acta Neuropathol *76*, 142-158.

Jones, P.L., Veenstra, G.J., Wade, P.A., Vermaak, D., Kass, S.U., Landsberger, N., Strouboulis, J., and Wolffe, A.P. (1998). Methylated DNA and MeCP2 recruit histone deacetylase to repress transcription. Nat Genet *19*, 187-191.

Jordan, C., Li, H.H., Kwan, H.C., and Francke, U. (2007). Cerebellar gene expression profiles of mouse models for Rett syndrome reveal novel MeCP2 targets. BMC Med Genet *8*, 36.

Jugloff, D.G., Vandamme, K., Logan, R., Visanji, N.P., Brotchie, J.M., and Eubanks, J.H. (2008). Targeted delivery of an Mecp2 transgene to forebrain neurons improves the behavior of female Mecp2-deficient mice. Hum Mol Genet *17*, 1386-396.

Kangaspeska, S., Stride, B., Métivier, R., Polycarpou-Schwarz, M., Ibberson, D., Carmouche, R.P., Benes, V., Gannon, F., and Reid, G. (2008). Transient cyclical methylation of promoter DNA. Nature *452*, 112-15.

Kaufmann, W.E., MacDonald, S.M., and Altamura, C.R. (2000). Dendritic cytoskeletal protein expression in mental retardation: an immunohistochemical study of the neocortex in Rett syndrome. Cereb Cortex *10*, 992-1004.

Kaufmann, W.E., Naidu, S., and Budden, S. (1995). Abnormal expression of microtubule-associated protein 2 (MAP-2) in neocortex in Rett syndrome. Neuropediatrics *26*, 109-113.

Kaufmann, W.E., Tierney, E., Rohde, C.A., Suarez-Pedraza, M.C., Clarke, M.A., Salorio, C.F., Bibat, G., Bukelis, I., Naram, D., et al. (2011). Social impairments in Rett syndrome: characteristics and relationship with clinical severity. J Intellect Disabil Res *56*, 233-247.

Kerr, A.M., Armstrong, D.D., Prescott, R.J., Doyle, D., and Kearney, D.L. (1997). Rett syndrome: analysis of deaths in the British survey. Eur Child Adolesc Psychiatry *6 Suppl 1*, 71-74.

Kerr, B., Soto C, J., Saez, M., Abrams, A., Walz, K., and Young, J.I. (2011). Transgenic complementation of MeCP2 deficiency: phenotypic rescue of Mecp2-null mice by isoform-specific transgenes. Eur J Hum Genet *20*, 69-76.

Kirby, R.S., Lane, J.B., Childers, J., Skinner, S.A., Annese, F., Barrish, J.O., Glaze, D.G., Macleod, P., and Percy, A.K. (2010). Longevity in Rett syndrome: analysis of the North American Database. J Pediatr *156*, 135-138.e1.

Kishi, N., and Macklis, J.D. (2004). MECP2 is progressively expressed in post-migratory neurons and is involved in neuronal maturation rather than cell fate decisions. Mol Cell Neurosci *27*, 306-321.

Kishi, N., and Macklis, J.D. (2009). MeCP2 functions largely cell-autonomously, but also non-cell-autonomously, in neuronal maturation and dendritic arborization of cortical pyramidal neurons. Exp Neurol 222, 51-58.

Klein, M.E., Lioy, D.T., Ma, L., Impey, S., Mandel, G., and Goodman, R.H. (2007). Homeostatic regulation of MeCP2 expression by a CREB-induced microRNA. Nat Neurosci *10*, 1513-14.

Kokura, K., Kaul, S.C., Wadhwa, R., Nomura, T., Khan, M.M., Shinagawa, T., Yasukawa, T., Colmenares, C., and Ishii, S. (2001). The Ski protein family is required for MeCP2-mediated transcriptional repression. J Biol Chem *276*, 34115-121.

Kriaucionis, S., and Bird, A. (2004). The major form of MeCP2 has a novel N-terminus generated by alternative splicing. Nucleic Acids Res *32*, 1818-823.

Kriaucionis, S., Paterson, A., Curtis, J., Guy, J., Macleod, N., and Bird, A. (2006). Gene expression analysis exposes mitochondrial abnormalities in a mouse model of Rett syndrome. Mol Cell Biol *26*, 5033-042.

Laurvick, C.L., de Klerk, N., Bower, C., Christodoulou, J., Ravine, D., Ellaway, C., Williamson, S., and Leonard, H. (2006). Rett syndrome in Australia: a review of the epidemiology. J Pediatr *148*, 347-352.

Lioy, D.T., Garg, S.K., Monaghan, C.E., Raber, J., Foust, K.D., Kaspar, B.K., Hirrlinger, P.G., Kirchhoff, F., Bissonnette, J.M., et al. (2011). A role for glia in the progression of Rett's syndrome. Nature 475, 497-500.

Liu, J., and Francke, U. (2006). Identification of cis-regulatory elements for MECP2 expression. Hum Mol Genet *15*, 1769-782.

Lonetti, G., Angelucci, A., Morando, L., Boggio, E.M., Giustetto, M., and Pizzorusso, T. (2010). Early environmental enrichment moderates the behavioral and synaptic phenotype of MeCP2 null mice. Biol Psychiatry *67*, 657-665.

Longair, M.H., Baker, D.A., and Armstrong, J.D. (2011). Simple Neurite Tracer: open source software for reconstruction, visualization and analysis of neuronal processes. Bioinformatics *27*, 2453-54.

Luikenhuis, S., Giacometti, E., Beard, C.F., and Jaenisch, R. (2004). Expression of MeCP2 in postmitotic neurons rescues Rett syndrome in mice. Proc Natl Acad Sci U S A *101*, 6033-38.

Lyon, M.F. (1961). Gene action in the X-chromosome of the mouse (Mus musculus L.). Nature *190*, 372-73.

Maezawa, I., and Jin, L.W. (2010). Rett syndrome microglia damage dendrites and synapses by the elevated release of glutamate. J Neurosci *30*, 5346-356.

Maezawa, I., Swanberg, S., Harvey, D., LaSalle, J.M., and Jin, L.W. (2009). Rett syndrome astrocytes are abnormal and spread MeCP2 deficiency through gap junctions. J Neurosci *29*, 5051-061.

Mari, F., Azimonti, S., Bertani, I., Bolognese, F., Colombo, E., Caselli, R., Scala, E., Longo, I., Grosso, S., et al. (2005). CDKL5 belongs to the same molecular pathway of

MeCP2 and it is responsible for the early-onset seizure variant of Rett syndrome. Hum Mol Genet *14*, 1935-946.

Matarazzo, V., Cohen, D., Palmer, A.M., Simpson, P.J., Khokhar, B., Pan, S.J., and Ronnett, G.V. (2004). The transcriptional repressor Mecp2 regulates terminal neuronal differentiation. Mol Cell Neurosci *27*, 44-58.

McGraw, C.M., Samaco, R.C., and Zoghbi, H.Y. (2011). Adult neural function requires MeCP2. Science *333*, 186.

Medrihan, L., Tantalaki, E., Aramuni, G., Sargsyan, V., Dudanova, I., Missler, M., and Zhang, W. (2008). Early defects of GABAergic synapses in the brain stem of a MeCP2 mouse model of Rett syndrome. J Neurophysiol *99*, 112-121.

Meehan, R.R., Lewis, J.D., and Bird, A.P. (1992). Characterization of MeCP2, a vertebrate DNA binding protein with affinity for methylated DNA. Nucleic Acids Res *20*, 5085-092.

Metcalf, B.M., Mullaney, B.C., Johnston, M.V., and Blue, M.E. (2006). Temporal shift in methyl-CpG binding protein 2 expression in a mouse model of Rett syndrome. Neuroscience *139*, 1449-460.

Miltenberger-Miltenyi, G., and Laccone, F. (2003). Mutations and polymorphisms in the human methyl CpG-binding protein MECP2. Hum Mutat *22*, 107-115.

Minks, J., and Brown, C.J. (2009). Getting to the center of X-chromosome inactivation: the role of transgenes. Biochem Cell Biol *87*, 759-766.

Miyake, K., and Nagai, K. (2007). Phosphorylation of methyl-CpG binding protein 2 (MeCP2) regulates the intracellular localization during neuronal cell differentiation. Neurochem Int *50*, 264-270.

Mnatzakanian, G.N., Lohi, H., Munteanu, I., Alfred, S.E., Yamada, T., MacLeod, P.J., Jones, J.R., Scherer, S.W., Schanen, N.C., et al. (2004). A previously unidentified MECP2 open reading frame defines a new protein isoform relevant to Rett syndrome. Nat Genet *36*, 339-341.

Nan, X., Campoy, F.J., and Bird, A. (1997). MeCP2 is a transcriptional repressor with abundant binding sites in genomic chromatin. Cell *88*, 471-481.

Nan, X., Ng, H.H., Johnson, C.A., Laherty, C.D., Turner, B.M., Eisenman, R.N., and Bird, A. (1998). Transcriptional repression by the methyl-CpG-binding protein MeCP2 involves a histone deacetylase complex. Nature *393*, 386-89.

Nan, X., Tate, P., Li, E., and Bird, A. (1996). DNA methylation specifies chromosomal localization of MeCP2. Mol Cell Biol *16*, 414-421.

Neul, J.L., Kaufmann, W.E., Glaze, D.G., Christodoulou, J., Clarke, A.J., Bahi-Buisson, N., Leonard, H., Bailey, M.E., Schanen, N.C., et al. (2010). Rett syndrome: Revised diagnostic criteria and nomenclature. Ann Neurol *68*, 944-950.

Nieuwenhuys, R. (1994). The neocortex. An overview of its evolutionary development, structural organization and synaptology. Anat Embryol (Berl) *190*, 307-337.

Nikitina, T., Ghosh, R.P., Horowitz-Scherer, R.A., Hansen, J.C., Grigoryev, S.A., and Woodcock, C.L. (2007). MeCP2-chromatin interactions include the formation of chromatosome-like structures and are altered in mutations causing Rett syndrome. J Biol Chem *282*, 28237-245.

Nuber, U.A., Kriaucionis, S., Roloff, T.C., Guy, J., Selfridge, J., Steinhoff, C., Schulz, R., Lipkowitz, B., Ropers, H.H., et al. (2005). Up-regulation of glucocorticoid-regulated genes in a mouse model of Rett syndrome. Hum Mol Genet *14*, 2247-256.

Okabe, Y., Kusaga, A., Takahashi, T., Mitsumasu, C., Murai, Y., Tanaka, E., Higashi, H., Matsuishi, T., and Kosai, K. (2010). Neural development of methyl-CpG-binding protein 2 null embryonic stem cells: a system for studying Rett syndrome. Brain Res *1360*, 17-27.

Okabe, Y., Takahashi, T., Mitsumasu, C., Kosai, K., Tanaka, E., and Matsuishi, T. (2012). Alterations of gene expression and glutamate clearance in astrocytes derived from an MeCP2-null mouse model of Rett syndrome. PLoS One *7*, e35354.

Parnavelas, J.G., Lieberman, A.R., and Webster, K.E. (1977). Organization of neurons in the visual cortex, area 17, of the rat. J Anat *124*, 305-322.

Pescucci, C., Meloni, I., Bruttini, M., Ariani, F., Longo, I., Mari, F., Canitano, R., Hayek, G., Zappella, M., and Renieri, A. (2003). Chromosome 2 deletion encompassing the MAP2 gene in a patient with autism and Rett-like features. Clin Genet *64*, 497-501.

Philippe, C., Villard, L., De Roux, N., Raynaud, M., Bonnefond, J.P., Pasquier, L., Lesca, G., Mancini, J., Jonveaux, P., et al. (2006). Spectrum and distribution of MECP2 mutations in 424 Rett syndrome patients: a molecular update. Eur J Med Genet *49*, 9-18.

Plenge, R.M., Stevenson, R.A., Lubs, H.A., Schwartz, C.E., and Willard, H.F. (2002). Skewed X-chromosome inactivation is a common feature of X-linked mental retardation disorders. Am J Hum Genet *71*, 168-173.

Prescott, T.E., Rødningen, O.K., Bjørnstad, A., and Stray-Pedersen, A. (2009). Two brothers with a microduplication including the MECP2 gene: rapid head growth in infancy and resolution of susceptibility to infection. Clin Dysmorphol *18*, 78-82.

Puck, J.M., and Willard, H.F. (1998). X inactivation in females with X-linked disease. N Engl J Med *338*, 325-28.

Reiss, A.L., Faruque, F., Naidu, S., Abrams, M., Beaty, T., Bryan, R.N., and Moser, H. (1993). Neuroanatomy of Rett syndrome: a volumetric imaging study. Ann Neurol *34*, 227-234.

Rett, A. (1966). [On a unusual brain atrophy syndrome in hyperammonemia in childhood]. Wien Med Wochenschr *116*, 723-26.

Robinson, L., Guy, J., McKay, L., Brockett, E., Spike, R.C., Selfridge, J., De Sousa, D., Merusi, C., Riedel, G., et al. (2012). Morphological and functional reversal of phenotypes in a mouse model of Rett syndrome. Brain *135*, 2699-2710.

Rodriguez, A., Ehlenberger, D., Kelliher, K., Einstein, M., Henderson, S.C., Morrison, J.H., Hof, P.R., and Wearne, S.L. (2003). Automated reconstruction of three-dimensional neuronal morphology from laser scanning microscopy images. Methods *30*, 94-105.

Ross, M.T., Grafham, D.V., Coffey, A.J., Scherer, S., McLay, K., Muzny, D., Platzer, M., Howell, G.R., Burrows, C., et al. (2005). The DNA sequence of the human X chromosome. Nature *434*, 325-337.

Samaco, R.C., Mandel-Brehm, C., Chao, H.T., Ward, C.S., Fyffe-Maricich, S.L., Ren, J., Hyland, K., Thaller, C., Maricich, S.M., et al. (2009). Loss of MeCP2 in aminergic neurons causes cell-autonomous defects in neurotransmitter synthesis and specific behavioral abnormalities. Proc Natl Acad Sci U S A *106*, 21966-971.

Samaco, R.C., McGraw, C.M., Ward, C.S., Sun, Y., Neul, J.L., and Zoghbi, H.Y. (2012). Female Mecp2+/- mice display robust behavioral deficits on two different genetic backgrounds providing a framework for pre-clinical studies. Hum Mol Genet.

Sandovici, I., Naumova, A.K., Leppert, M., Linares, Y., and Sapienza, C. (2004). A longitudinal study of X-inactivation ratio in human females. Hum Genet *115*, 387-392.

Santos, M., Silva-Fernandes, A., Oliveira, P., Sousa, N., and Maciel, P. (2007). Evidence for abnormal early development in a mouse model of Rett syndrome. Genes Brain Behav *6*, 277-286.

Saywell, V., Viola, A., Confort-Gouny, S., Le Fur, Y., Villard, L., and Cozzone, P.J. (2006). Brain magnetic resonance study of Mecp2 deletion effects on anatomy and metabolism. Biochem Biophys Res Commun *340*, 776-783.

Schnell, S.A., Staines, W.A., and Wessendorf, M.W. (1999). Reduction of Lipofuscin-like Autofluorescence in Fluorescently Labeled Tissue. Journal of Histochemistry & Cytochemistry *47*, 719.

Schüle, B., Armstrong, D.D., Vogel, H., Oviedo, A., and Francke, U. (2008). Severe congenital encephalopathy caused by MECP2 null mutations in males: central hypoxia and reduced neuronal dendritic structure. Clin Genet *74*, 116-126.

Scorcioni, R., Lazarewicz, M.T., and Ascoli, G.A. (2004). Quantitative morphometry of hippocampal pyramidal cells: differences between anatomical classes and reconstructing laboratories. J Comp Neurol *473*, 177-193.

Scorcioni, R., Polavaram, S., and Ascoli, G.A. (2008). L-Measure: a web-accessible tool for the analysis, comparison and search of digital reconstructions of neuronal morphologies. Nat Protoc *3*, 866-876.

Shahbazian, M., Young, J., Yuva-Paylor, L., Spencer, C., Antalffy, B., Noebels, J., Armstrong, D., Paylor, R., and Zoghbi, H. (2002). Mice with truncated MeCP2 recapitulate many Rett syndrome features and display hyperacetylation of histone H3. Neuron *35*, 243-254.

Shahbazian, M.D., Antalffy, B., Armstrong, D.L., and Zoghbi, H.Y. (2002). Insight into Rett syndrome: MeCP2 levels display tissue- and cell-specific differences and correlate with neuronal maturation. Hum Mol Genet *11*, 115-124.

Sharp, A., Robinson, D., and Jacobs, P. (2000). Age-and tissue-specific variation of X chromosome inactivation ratios in normal women. Hum Genet *107*, 343-49.

Sholl, D.A. (1953). Dendritic organization in the neurons of the visual and motor cortices of the cat. J Anat *87*, 387-405.

Singleton, M.K., Gonzales, M.L., Leung, K.N., Yasui, D.H., Schroeder, D.I., Dunaway, K., and LaSalle, J.M. (2011). MeCP2 is required for global heterochromatic and nucleolar changes during activity-dependent neuronal maturation. Neurobiol Dis *43*, 190-200.

Sirianni, N., Naidu, S., Pereira, J., Pillotto, R.F., and Hoffman, E.P. (1998). Rett syndrome: confirmation of X-linked dominant inheritance, and localization of the gene to Xq28. Am J Hum Genet *63*, 1552-58.

Skene, P.J., Illingworth, R.S., Webb, S., Kerr, A.R., James, K.D., Turner, D.J., Andrews, R., and Bird, A.P. (2010). Neuronal MeCP2 is expressed at near histone-octamer levels and globally alters the chromatin state. Mol Cell *37*, 457-468.

Smrt, R.D., Eaves-Egenes, J., Barkho, B.Z., Santistevan, N.J., Zhao, C., Aimone, J.B., Gage, F.H., and Zhao, X. (2007). Mecp2 deficiency leads to delayed maturation and altered gene expression in hippocampal neurons. Neurobiol Dis *27*, 77-89.

Smrt, R.D., Pfeiffer, R.L., and Zhao, X. (2011). Age-dependent expression of MeCP2 in a heterozygous mosaic mouse model. Hum Mol Genet *20*, 1834-843.

Stuss, D.P., Boyd, J.D., Levin, D.B., and Delaney, K.R. (2012). MeCP2 Mutation Results in Compartment-Specific Reductions in Dendritic Branching and Spine Density in Layer 5 Motor Cortical Neurons of YFP-H Mice. PLoS One *7*, e31896.

Subramaniam, B., Naidu, S., and Reiss, A.L. (1997). Neuroanatomy in Rett syndrome: cerebral cortex and posterior fossa. Neurology *48*, 399-407.

Taneja, P., Ogier, M., Brooks-Harris, G., Schmid, D.A., Katz, D.M., and Nelson, S.B. (2009). Pathophysiology of locus ceruleus neurons in a mouse model of Rett syndrome. J Neurosci *29*, 12187-195.

Tao, J., Hu, K., Chang, Q., Wu, H., Sherman, N.E., Martinowich, K., Klose, R.J., Schanen, C., Jaenisch, R., et al. (2009). Phosphorylation of MeCP2 at Serine 80 regulates its chromatin association and neurological function. Proc Natl Acad Sci U S A *106*, 4882-87.

Tao, J., Van Esch, H., Hagedorn-Greiwe, M., Hoffmann, K., Moser, B., Raynaud, M., Sperner, J., Fryns, J.P., Schwinger, E., et al. (2004). Mutations in the X-linked cyclin-dependent kinase-like 5 (CDKL5/STK9) gene are associated with severe neurodevelopmental retardation. Am J Hum Genet *75*, 1149-154.

Thomson, A.M., Bannister, A.P., Mercer, A., and Morris, O.T. (2002). Target and temporal pattern selection at neocortical synapses. Philos Trans R Soc Lond B Biol Sci *357*, 1781-791.

Trappe, R., Laccone, F., Cobilanschi, J., Meins, M., Huppke, P., Hanefeld, F., and Engel, W. (2001). MECP2 mutations in sporadic cases of Rett syndrome are almost exclusively of paternal origin. Am J Hum Genet *68*, 1093-1101.

Vo, N., Klein, M.E., Varlamova, O., Keller, D.M., Yamamoto, T., Goodman, R.H., and Impey, S. (2005). A cAMP-response element binding protein-induced microRNA regulates neuronal morphogenesis. Proc Natl Acad Sci U S A *102*, 16426-431.

Watts, J., and Thomson, A.M. (2005). Excitatory and inhibitory connections show selectivity in the neocortex. J Physiol *562*, 89-97.

Wayman, G.A., Davare, M., Ando, H., Fortin, D., Varlamova, O., Cheng, H.Y., Marks, D., Obrietan, K., Soderling, T.R., et al. (2008). An activity-regulated microRNA controls dendritic plasticity by down-regulating p250GAP. Proc Natl Acad Sci U S A *105*, 9093-98.

Wearne, S.L., Rodriguez, A., Ehlenberger, D.B., Rocher, A.B., Henderson, S.C., and Hof, P.R. (2005). New techniques for imaging, digitization and analysis of three-dimensional neural morphology on multiple scales. Neuroscience *136*, 661-680.

Weaving, L.S., Christodoulou, J., Williamson, S.L., Friend, K.L., McKenzie, O.L., Archer, H., Evans, J., Clarke, A., Pelka, G.J., et al. (2004). Mutations of CDKL5 cause a severe neurodevelopmental disorder with infantile spasms and mental retardation. Am J Hum Genet *75*, 1079-093.

Weaving, L.S., Ellaway, C.J., Gécz, J., and Christodoulou, J. (2005). Rett syndrome: clinical review and genetic update. J Med Genet *42*, 1-7.

Weng, S.M., McLeod, F., Bailey, M.E., and Cobb, S.R. (2011). Synaptic plasticity deficits in an experimental model of rett syndrome: long-term potentiation saturation and its pharmacological reversal. Neuroscience *180*, 314-321.

Yasui, D.H., Peddada, S., Bieda, M.C., Vallero, R.O., Hogart, A., Nagarajan, R.P., Thatcher, K.N., Farnham, P.J., and Lasalle, J.M. (2007). Integrated epigenomic analyses of neuronal MeCP2 reveal a role for long-range interaction with active genes. Proc Natl Acad Sci U S A *104*, 19416-421.

Yazdani, M., Deogracias, R., Guy, J., Poot, R.A., Bird, A., and Barde, Y.A. (2012). Disease Modeling Using Embryonic Stem Cells: MeCP2 Regulates Nuclear Size and RNA Synthesis in Neurons. Stem Cells *30*, 2128-139.

Young, J.I., and Zoghbi, H.Y. (2004). X-chromosome inactivation patterns are unbalanced and affect the phenotypic outcome in a mouse model of rett syndrome. Am J Hum Genet *74*, 511-520.

Young, J.I., Hong, E.P., Castle, J.C., Crespo-Barreto, J., Bowman, A.B., Rose, M.F., Kang, D., Richman, R., Johnson, J.M., et al. (2005). Regulation of RNA splicing by the methylation-dependent transcriptional repressor methyl-CpG binding protein 2. Proc Natl Acad Sci U S A *102*, 17551-58.

Zappella, M., Meloni, I., Longo, I., Canitano, R., Hayek, G., Rosaia, L., Mari, F., and Renieri, A. (2003). Study of MECP2 gene in Rett syndrome variants and autistic girls. Am J Med Genet B Neuropsychiatr Genet *119B*, 102-07.

Zappella, M., Meloni, I., Longo, I., Hayek, G., and Renieri, A. (2001). Preserved speech variants of the Rett syndrome: molecular and clinical analysis. Am J Med Genet *104*, 14-22.

Zhang, L., He, J., Jugloff, D.G., and Eubanks, J.H. (2008). The MeCP2-null mouse hippocampus displays altered basal inhibitory rhythms and is prone to hyperexcitability. Hippocampus *18*, 294-309.

Zhou, Z., Hong, E.J., Cohen, S., Zhao, W.N., Ho, H.Y., Schmidt, L., Chen, W.G., Lin, Y., Savner, E., et al. (2006). Brain-specific phosphorylation of MeCP2 regulates activity-dependent Bdnf transcription, dendritic growth, and spine maturation. Neuron *52*, 255-269.